AGU PUBLICATIONS

Geochemistry, Geophysics, Geosystems

RESEARCH ARTICLE
10.1002/2015GC005723

Mantle plume capture, anchoring, and outflow during Galápagos plume-ridge interaction

S. A. Gibson[1], D. J. Geist[2], and M. A. Richards[3]

[1]Department of Earth Sciences, University of Cambridge, Cambridge, UK, [2]Department of Geological Sciences, University of Idaho, Moscow, Idaho, USA, [3]Department of Earth and Planetary Science, University of California, Berkeley, California, USA

Key Points:
- Recycled oceanic crust contributes to Galapagos Spreading Center basalts
- On-axis capture and anchoring of Galapagos plume stem during ridge migration
- Deep melt channels may connect Galapagos plume and adjacent ridge

Supporting Information:
- Supporting Information S1

Correspondence to:
S. A. Gibson,
sally@esc.cam.ac.uk

Citation:
Gibson, S. A., D. J. Geist, and M. A. Richards (2015), Mantle plume capture, anchoring, and outflow during Galápagos plume-ridge interaction, *Geochem. Geophys. Geosyst.*, *16*, doi:10.1002/2015GC005723.

Received 14 JAN 2015
Accepted 17 APR 2015
Accepted article online 24 APR 2015

Abstract Compositions of basalts erupted between the main zone of Galápagos plume upwelling and adjacent Galápagos Spreading Center (GSC) provide important constraints on dynamic processes involved in transfer of deep-mantle-sourced material to mid-ocean ridges. We examine recent basalts from central and northeast Galápagos including some that have less radiogenic Sr, Nd, and Pb isotopic compositions than plume-influenced basalts (E-MORB) from the nearby ridge. We show that the location of E-MORB, greatest crustal thickness, and elevated topography on the GSC correlates with a confined zone of low-velocity, high-temperature mantle connecting the plume stem and ridge at depths of ~100 km. At this site on the ridge, plume-driven upwelling involving deep melting of partially dehydrated, recycled ancient oceanic crust, plus plate-limited shallow melting of anhydrous peridotite, generate E-MORB and larger amounts of melt than elsewhere on the GSC. The first-order control on plume stem to ridge flow is rheological rather than gravitational, and strongly influenced by flow regimes initiated when the plume was on axis (>5 Ma). During subsequent northeast ridge migration material upwelling in the plume stem appears to have remained "anchored" to a contact point on the GSC. This deep, confined NE plume stem-to-ridge flow occurs via a network of melt channels, embedded within the normal spreading and advection of plume material beneath the Nazca plate, and coincides with locations of historic volcanism. Our observations require a more dynamically complex model than proposed by most studies, which rely on radial solid-state outflow of heterogeneous plume material to the ridge.

1. Introduction

Sites of plume-ridge interaction correspond to some of the world's most active volcanism, but the dynamic processes involved in the transfer of compositionally distinct material from a deep-seated mantle plume to an adjacent spreading ridge are not fully understood. The restricted spatial extents of geophysical and geochemical data together with tectonic complexities at sites of off-axis plume-ridge interaction limit our understanding of the underlying mass transfer processes and interpretations are largely based on the findings of numerical and laboratory studies. In situations where the ridge migrates away from the hot spot, major outstanding problems concern (i) the lateral extent of plume outflow in the upper mantle, which relates to models of dispersal of high-temperature material away from the plume stem, e.g., by radial outflow or basal lithospheric channeling [*Schilling*, 1991; *Feighner and Richards*, 1995; *Kincaid et al*., 1995; *Small*, 1995; *Kingsley and Schilling*, 1998; *Ribe and Delattre*, 1998; *Sleep*, 2008] and (ii) the nature of the boundary layer that controls the depth of flow. Whereas some workers advocate a significant role for gravitational flow of plume material upslope, along the base of the lithosphere, toward the adjacent ridge [*Schilling et al*., 1985; *Schilling*, 1991; *Kincaid et al*., 1996; *Kingsley and Schilling*, 1998; *Sleep*, 2002, 2008; *Braun and Sohn*, 2003], others favor ridgeward horizontal flow at depths well below the anhydrous peridotite solidus [*Ribe*, 1996; *Ito et al*., 1997, 1999; *Hall and Kincaid*, 2003, 2004; *Villagómez et al*., 2014].

Our study of plume-ridge interaction is focused on the Galápagos Archipelago and adjacent Galápagos Spreading Center (GSC) (Figure 1). This region is exceptional because the islands are widely distributed between the upwelling plume and adjacent intermediate-spreading ridge (Figure 1), and the compositions of recently erupted basalts provide a broad aperture into underlying mantle processes. Also, there are high-resolution seismic data from which to constrain spatial variations in lithospheric thickness, melt distribution, and temperature [*Villagómez et al*., 2007, 2011, 2014; *Gibson and Geist*, 2010; *Byrnes et al*., 2015]. At least five

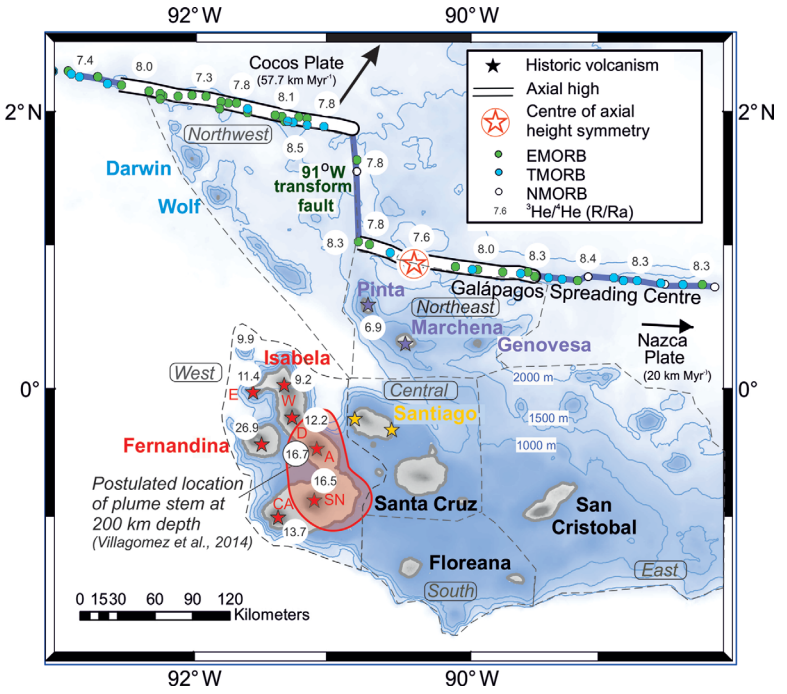

Figure 1. Spatial relationship of the Galápagos hot spot to the Galápagos spreading center (GSC). The GSC is an intermediate spreading-ridge along which the full spreading rate varies from 40 mm/yr in the west to 65 mm/yr in the east [*DeMets et al*., 1994]. Open star in circle at 90.42°W represents the center of symmetry of the isostatic axial depth profile [*Ito et al*., 1997]. Subdivisions of basalt types from the GSC, based on K/Ti ratios, are from *Schilling et al*. [1982, 2003], *Detrick et al*. [2002], *Cushman et al*. [2004], *Christie et al*. [2005], and *Ingle et al*. [2010]. $^{3}He/^{4}He$ (R/Ra) for volcanoes that have experienced historic eruptions are from *Graham et al*. [1993, 2014], *Kurz and Geist* [1999], and *Kurz et al*. [2010]. A, CA, D, E, SN, and W show the locations of the Alcedo, Cerro Azul, Darwin, Ecuador, Sierra Negra, and Wolf volcanoes on Isabela, respectively. Plate velocities and vectors are from *Gripp and Gordon* [2002]. Galápagos subprovinces are after *Geist et al*. [1998] and color coding illustrates locations mentioned in the text and geochemical plots.

different models of plume-ridge interaction have been proposed for Galápagos. These include: (i) flow of plume material in a sublithospheric channel [*Morgan*, 1978; *Schilling et al*., 1982; *Verma and Schilling*, 1982; *Braun and Sohn*, 2003]; (ii) a spreading "puddle" model involving radial flow away from the plume stem [*Schilling et al*., 1982; *Shorttle et al*., 2010]; (iii) eastward bending of the plume head in the direction of motion of the Nazca Plate [*Richards and Griffiths*, 1989; *Geist*, 1992; *White et al*., 1993; *Harpp and White*, 2001]; (iv) gravitational spreading along the base of the lithosphere [*Bercovici and Lin*, 1996]; and (v) solid-state transport of plume material beneath a dehydrated, high-viscosity mantle lid [*Kokfelt et al*., 2005; *Ito and Bianco*, 2014; *Villagómez et al*., 2014; *Byrnes et al*., 2015].

We use geochemical and geophysical observables for the Galápagos Archipelago and adjacent spreading center together with inferences from published fluid mechanical models to assess the mechanisms involved in the mass transfer of plume material to the ridge. Important to our interpretations are recently published geochemical data sets for islands in central and NE Galápagos [*Gibson et al*., 2012; *Harpp et al*., 2014b]. Basalts from these islands have low $^{87}Sr/^{86}Sr$ and high $^{143}Nd/^{144}Nd$ isotopic ratios relative to those on the nearest section of ridge and contain a greater contribution of melts derived from a depleted mantle source. We show that covariations in Pb isotopes are evidence that ancient recycled oceanic crust contributes to these basalts and also those erupted on the adjacent spreading ridge. Moreover, we have identified a mechanism by which the capture of material upwelling in the on-axis Galápagos plume stem by the GSC is maintained during subsequent ridge migration and remains anchored to a contact point on the spreading axis. This causes a deep confined zone of long-term plume stem-to-ridge flow embedded within "normal" spreading of material in the plume head.

2. Melt Generation Beneath Galápagos

2.1. Mantle Reservoirs Intrinsic to the Galápagos Plume

Regional investigations of basalts from the Galápagos Archipelago have shown that they result from melting of at least four isotopically distinct reservoirs intrinsic to a mantle plume [*Geist et al*., 1988; *White et al*.,

Table 1. Summary of Compositional Variations Exhibited by Basalts From the Galápagos Archipelago and Spreading Center

	$[La/Sm]_n$		$[Sm/Yb]_n$		$[La/Nb]_n$		$^{87}Sr/^{86}Sr$		εNd		$^{206}Pb/^{204}Pb$		$^{207}Pb/^{204}Pb$		$^{208}Pb/^{204}Pb$	
	$\bar{X}$	σ	$\bar{X}$	σ	$\bar{X}$	σ	$\bar{X}$	σ	$\bar{X}$	σ	$\bar{X}$	σ	$\bar{X}$	σ	$\bar{X}$	σ
Western Galápagos																
Fernandina	1.55	0.06	2.62	1.02	0.64	0.16	0.70323	0.00004	5.86	0.23	19.08	0.02	15.55	0.01	38.71	0.04
Central Galápagos (Santiago)																
Mildly-alkaline basalts	1.50	0.13	2.42	0.32	0.82	0.06	0.70302	0.00024	7.07	0.28	19.12	0.09	15.59	0.00	38.75	0.08
Transitional basalts	1.17	0.18	1.75	0.27	1.04	0.13	0.70284	0.00004	7.99	0.52	18.77	0.15	15.55	0.02	38.36	0.15
Low-K MORB-like tholeiites	0.80	0.07	1.12	0.13	1.12	0.10	0.70285	0.00009	8.25	0.42	18.66	0.06	15.54	0.01	38.24	0.06
Northeast Galápagos																
Genovesa	0.49	0.08	1.13	0.14	1.58	0.12	0.70267	0.00005	9.52	0.25	18.44	0.07	15.53	0.03	38.02	0.12
Marchena	0.89	0.05	1.60	0.13	0.81		0.70282	0.00005	7.78	0.17	18.91	0.02	15.56	0.00	38.51	0.01
Pinta	2.36	0.24	2.30	0.3	0.72	0.06	0.70326	0.00010	5.33	0.52	19.22	0.09	15.61	0.02	39.13	0.14
Western Galápagos Spreading Center																
E-MORB	1.37	0.16	1.45	0.40	0.67	0.24	0.70296	0.00006	7.52	0.56	18.82	0.11	15.56	0.01	38.61	0.11
T-MORB	0.91	0.32	1.09	0.30	0.77	0.11	0.70291	0.00008	7.52	0.56	18.82	0.11	15.56	0.01	38.61	0.11
N-MORB	0.57	0.10	0.97	0.09	1.20	0.28	0.70273	0.00015	8.52	0.92	18.56	0.17	15.53	0.02	38.29	0.19
Eastern Galápagos Spreading Center																
E-MORB	0.93	0.44	1.23	0.26	0.78	0.25	0.70282	0.00011	7.92	1.25	18.89	0.26	15.57	0.04	38.56	0.35
T-MORB	0.78	0.07	1.11	0.11	0.81	0.06	0.70274	0.00017	8.48	1.06	18.75	0.14	15.55	0.03	38.40	0.22
N-MORB	0.57	0.11	0.98	0.11	1.22	0.58	0.70263	0.00026	9.04	0.72	18.54	0.21	15.52	0.04	38.10	0.28

[a]Data are from *Schilling et al.* [1982, 2003], *White et al.* [1993], *Christie et al.* [2005], *Saal et al.* [2007], *Gibson et al.* [2012], and *Harpp et al.* [2014b].

1993; *Hoernle et al.*, 2000; *Blichert-Toft and White*, 2001; *Harpp and White*, 2001]. Across the Archipelago, melt contributions from these different Galápagos plume reservoirs correlate with lithospheric thickness [*Gibson and Geist*, 2010]. In this work, we exploit this long wavelength spatial variability of isotopically distinct plume reservoirs to infer the flow of Galápagos plume material.

The high $^3He/^4He$, $^{87}Sr/^{86}Sr$ and low $^{143}Nd/^{144}Nd$ Galápagos plume (PLUME) reservoir shares the high Ti, Ta, and Nb compositions of other hot spot provinces [*Jackson et al.*, 2008] and isotopically resembles the global mantle plume component known as FOZO or C [*Hart et al.*, 1992; *Hanan and Graham*, 1996]. PLUME is most dominant in basalts from western Galápagos, i.e., Fernandina and Isabela, above the zone of greatest mantle plume upwelling [*Kurz and Geist*, 1999]. Other Galápagos plume reservoirs with relatively radiogenic Sr, Nd, and Pb isotopic compositions include Floreana (FLO) and Wolf-Darwin (WD), which are prevalent in basalts erupted in southern and northwestern Galápagos, respectively. FLO has a similar Nd isotopic ratio to the PLUME reservoir, intermediate $^3He/^4He$ together with high $^{87}Sr/^{86}Sr$ and elevated $^{206}Pb/^{204}Pb$ ratios, and has recently been interpreted as ancient (>2 Ga) altered oceanic crust [*Harpp et al.*, 2014a]. WD is distinguished from other Galápagos plume reservoirs by elevated $^{208}Pb/^{204}Pb$ at a given $^{206}Pb/^{204}Pb$ ratio and may represent an ancient sedimentary component within the plume [*Schilling et al.*, 2003]. The Galápagos mantle plume reservoir with relatively unradiogenic Sr, Nd, and Pb isotopic compositions, which we refer to here as Depleted Galápagos mantle (DGM), tends to be more evident in basalts erupted on thinner lithosphere in northeast Galápagos (Genovesa) and in central and eastern parts of the archipelago (e.g., eastern Santiago, Santa Cruz, and San Cristobal). The Pb isotopic composition of DGM is subtly different from the global MORB source [*Ingle et al.*, 2010]. While the extent of lithological variations in the Galápagos plume remains uncertain, the dominant source material in the Galápagos plume is believed to be peridotite [*Vidito et al.*, 2013], with recycled ancient oceanic crust (FLO) and sediment (WD) making only small contributions to erupted melts [*Harpp and White*, 2001].

2.2. Western Galápagos: Plume Stem Melts

The most voluminous volcanism occurs in western Galápagos in the vicinity of the present-day plume stem, which has been imaged as a steeply dipping low seismic-velocity anomaly in the upper mantle in tomographic studies [*Villagómez et al.*, 2014] (Figure 1). Lavas on the islands of Fernandina and southern Isabela are characterized by the highest $^3He/^4He$ (up to 29 R/Ra) and lowest $^{143}Nd/^{144}Nd$ and $[La/Nb]_n$ ratios of any Galápagos basalts [*Graham et al.*, 1993; *Kurz and Geist*, 1999; *Geist et al.*, 2006; *Saal et al.*, 2007; *Kurz et al.*, 2009] (Table 1 and Figure 2). Western Galápagos basalts have the highest $[Sm/Yb]_n$ ratios, which correlate with a thick lithosphere (55–60 km) [*Gibson and Geist*, 2010]. Small variations in elemental and isotopic ratios have been linked to short wavelength variations in plume composition [*Geist et al.*, 2005].

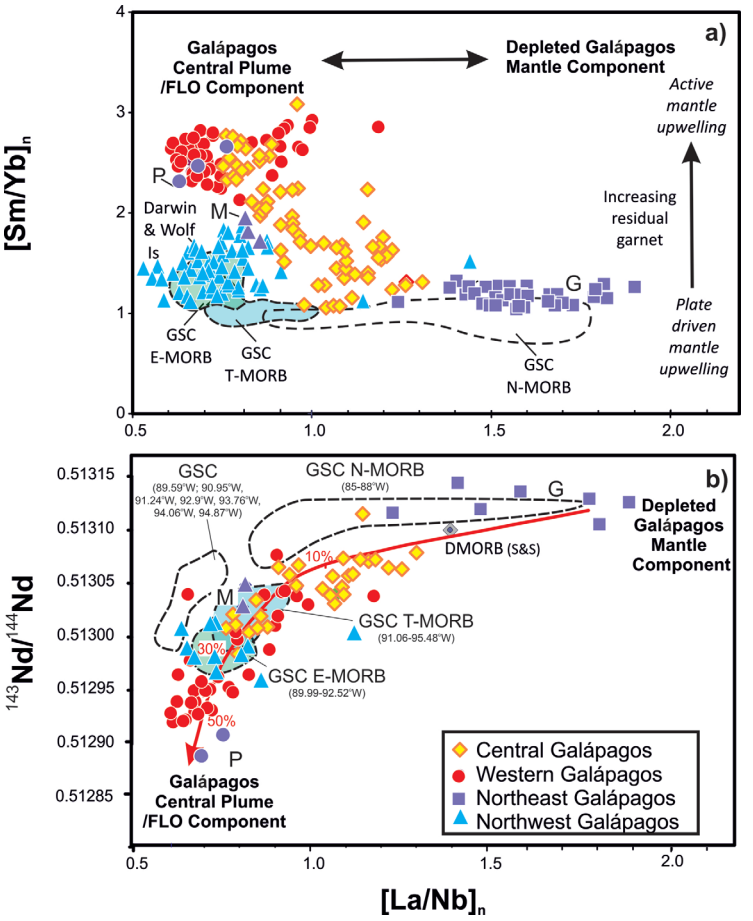

Figure 2. Variation of $[La/Nb]_n$ with $^{143}Nd/^{144}Nd$ and $[Sm/Yb]_n$ ratios in basalts from the Galápagos archipelago and adjacent Galápagos Spreading Center (GSC). Plots exclude basalts identified by *Harpp and White* [2001] as having a high Floreana incompatible trace element and isotopically enriched mantle component. G, M, and P correspond to Genovesa, Marchena, and Pinta, respectively. (a) Variation of $[La/Nb]_n$ with $[Sm/Yb]_n$. Note that basalts from Wolf and Darwin Islands have similar $[La/Nb]_n$ and $[Sm/Yb]_n$ to E-MORB whereas those from Genovesa (diamonds) are comparable to NMORB. (b) The solid red arrow illustrates binary mixing between melts from a depleted end-member, that has the composition of a Genovesa basalt (and similar to average depleted MORB, D-MORB), with an enriched end-member melt, similar in composition to Floreana basalts [*Harpp and White*, 2001]. If melts are also derived from the enriched PLUME source then estimates for DGM are maximum values. Note that N-MORB and some T-MORB and E-MORB from the western GSC plot well above the mixing curve. Normalization factors are from *McDonough and Sun* [1995]. Data are from *Schilling et al.* [1982, 2003], *White et al.* [1993], *Harpp and White* [2001], *Detrick et al.* [2002], *Harpp and Geist* [2002], *Harpp et al.* [2003], *Cushman et al.* [2004], *Christie et al.* [2005], *Fitton* [2007], *Saal et al.* [2007], *Gibson and Geist* [2010], *Ingle et al.* [2010], and *Harpp et al.* [2014b].

2.3. Central and Northern Galápagos: Sampling Melts of Plume Outflow

Historic volcanism has also occurred in central Galápagos on Santiago, beyond the margin of the plume stem (Figure 1). Santiago lavas range in composition from low-K tholeiites to mildly alkaline basalts and exhibit strikingly large variations in incompatible trace element and isotopic ratios in comparison to those from the western and northern Galápagos Islands [*Gibson et al.*, 2012] (Figure 2). Large variations of $[Sm/Yb]_n$ in basalts from Isla Santiago, over a distance of 20 km, coincide with a major 10 km lithospheric "step" beneath the island [*Gibson et al.*, 2012]. Older, but compositionally similar basalts also erupt from Islas Santa Cruz and San Cristobal.

Much of the region between the plume stem and the closest segment of spreading ridge is >1000 m below sea level and melts of plume material undergoing ridgeward flow are sampled by tholeiitic basalts erupted on Islas Wolf, Darwin, Pinta, Marchena, and Genovesa together with seamounts in northern Galápagos [*Harpp and White*, 2001; *Harpp et al.*, 2014b]. Basalts from Pinta have similar $[Sm/Yb]_n$, $[La/Nb]_n$, and $^{143}Nd/^{144}Nd$ ratios (although distinctive Pb and Sr isotopic ratios) to enriched basalts in western Galápagos whereas other basalts from northeast Galápagos (Marchena and Genovesa) are comparable to basalts erupted in central Galápagos, i.e., on western and eastern Santiago, respectively (Table 1 and Figure 2). Basalts erupted in northwest Galápagos (Islas Wolf and Darwin) are notable for their low $[La/Nb]_n$ and elevated $^{208}Pb/^{204}Pb$ ratios, which are a distinctive feature of the PLUME and WD reservoirs, respectively [*Harpp and White*, 2001; *Harpp et al.*, 2014b].

2.4. Galápagos Spreading Center: Plume Melting Beneath the Ridge

The morphology and geochemistry of the GSC indicate that the maximum influence of the Galápagos hot spot occurs across a broad region centered on 90.5°W, but the pattern is complicated by the Galápagos 91°W transform fault [e.g., *Schilling et al.*, 1976, 1982, 2003; *Ito et al.*, 1997; *Canales et al.*, 2002] (Figure 1).

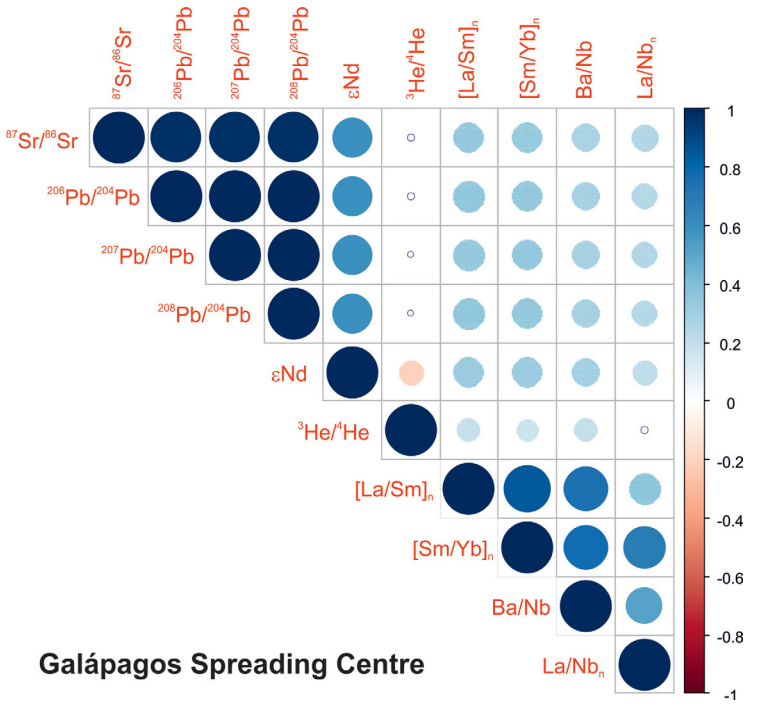

Figure 3. Correlation matrix of isotopic and incompatible trace element ratios for Galápagos Spreading Center basalts. The moderate correlation between isotopic and incompatible trace element ratios in GSC basalts suggests that variability in source compositions and the depths and extents of melting are imperfectly coupled. This highlights the complexity of chemical and physical processes during plume-ridge interactions. Data used in correlations are from *Schilling et al.* [1982, 2003], *Detrick et al.* [2002], *Cushman et al.* [2004], *Christie et al.* [2005], *Ingle et al.* [2010], and *Graham et al.* [1993, 2014].

The GSC geochemical anomaly is most prominent between ~92.5°W and 89.5°W, where the erupted basalts resemble global enriched (E-) MORB, i.e., they typically have elevated K/Ti and light rare earth element concentrations together with relatively high $[La/Sm]_n$, [Sm/Yb] and $[La/Nb]_n$, and εNd values as low as 5.6 [*Schilling et al.*, 1982, 2003; *Ito and Lin*, 1995a; *Ito et al.*, 1997; *Canales et al.*, 2002; *Detrick et al.*, 2002; *Cushman et al.*, 2004; *Christie et al.*, 2005; *Kokfelt et al.*, 2005; *Ingle et al.*, 2010]. The location of E-MORB corresponds to axial highs on both the eastern and western GSC (Figure 1). Transitional (T-) MORBs with moderate K/Ti, $[Sm/Yb]_n$, $[La/Nb]_n$, and εNd values tend to occur on the GSC either side of E-MORBs where the ridge is at a similar or lower elevation (Figure 1). Normal (N-) MORBs with low K/Ti and high $[La/Nb]_n$ are found at the eastern and western ends of plume-influenced ridge and are associated with an axial low.

Subtle differences exist in some incompatible trace element ratios and also the isotopic ratios of MORBs erupted on the eastern and western GSC [*Schilling et al.*, 1982, 2003; *Ito and Lin*, 1995a; *Ito et al.*, 1997; *Canales et al.*, 2002; *Detrick et al.*, 2002; *Cushman et al.*, 2004; *Christie et al.*, 2005; *Kokfelt et al.*, 2005; *Ingle et al.*, 2010]. In particular, E-MORBs from the eastern GSC have lower La/Sm, Ba/Nb, Nb/Zr, $^{87}Sr/^{86}Sr$, $^{207}Pb/^{204}Pb$, $^{208}Pb/^{204}Pb$, and $^{230}Th/^{238}U$ ratios and higher $^{206}Pb/^{204}Pb$, $^{143}Nd/^{144}Nd$, $^{176}Hf/^{177}Hf$, and $^{3}He/^{4}He$ than E-MORBs on the western GSC. These differences are important because they suggest that different mantle reservoirs, intrinsic to the Galápagos plume, are melting beneath different sections of the ridge. While there is no significant correlation between $^{3}He/^{4}He$ and Sr, Nd, and Pb isotopic ratios (Figure 3) in GSC basalts, the along axis gradient in all of these isotopic ratios is unaffected by the 91°W transform fault [*Graham et al.*, 2014]. All GSC basalts are characterized by low $^{3}He/^{4}He$ (Figure 1) and the decoupling (and also of CO_2, $^{21}Ne/^{22}Ne$, and $^{4}He/^{40}Ar$) from Sr, Nd, and Pb isotopic ratios has been attributed to depletion of highly volatile elements during deep melting in the Galápagos plume stem [*Villagómez et al.*, 2014].

2.5. Variable Melting of Recycled Oceanic Crust in the Galápagos Archipelago and Adjacent Ridge

The different correlations between $[La/Nb]_n$ and $[Sm/Yb]_n$ in basalts from the GSC compared to those in the Galápagos Archipelago (excluding Wolf and Darwin Is; Figure 2) occur primarily because the various types of GSC MORB exhibit large differences in proportions of low $[La/Nb]_n$, isotopically enriched (PLUME, FLO,

and WD components) and high $[La/Nb]_n$ isotopically depleted Galápagos mantle (DGM) plume-derived melts but show relatively minor variations in $[Sm/Yb]_n$ compared to those in the archipelago (Table 1).

It was previously thought that the isotopically enriched FLO component (partially dehydrated ancient recycled oceanic crust) was restricted to the southern Galapagos Archipelago [*Harpp and White*, 2001] but recently published isotopic data for central Galápagos basalts (Isla Santiago) [*Gibson et al*., 2012] provide important constraints on how this deep-sourced plume material is dispersed toward the ridge. This is because Santiago basalts exhibit far greater isotopic variations than any other island in the archipelago. When combined with data for northeast and western Galápagos [*White et al*., 1993; *Saal et al*., 2007], Santiago compositions display continuous linear variations between recycled ancient oceanic crust (FLO) and depleted mantle (DGM) in isotopic space (Figure 4).

In order to quantitatively and statistically assess the mixing relations, principal component analysis (PCA) is applied to isotopic data from all of the islands and the GSC (see supporting information). PCA shows that variance in all Galapagos Island and GSC isotopic data can be explained by five vectors (Table S1), following *Harpp and White* [2001]. The first three principal components account for ~76%, 12%, and 8% of the variance, respectively, whereas PC4 and PC5 are so small (<4%) that they are insignificant. The first principal component vector (PC1) defines mixing between high $^{208}Pb/^{206}Pb$, $^{207}Pb/^{206}Pb$ DGM and low $^{208}Pb/^{206}Pb$, $^{207}Pb/^{206}Pb$ FLO mantle. The second component vector (PC2) extends toward the PLUME component. The third component vector (PC3) involves a fourth end-member with moderate $^{208}Pb/^{206}Pb$, $^{207}Pb/^{206}Pb$ and high $^{208}Pb/^{207}Pb$ and resembles WD (ancient recycled sediment). PC3 is most prevalent in E-MORB and T-MORB on the western GSC.

In order to eliminate errors associated with the common ^{204}Pb isotope, we have illustrated variations on $^{208}Pb/^{206}Pb$ versus $^{207}Pb/^{206}Pb$ and $^{208}Pb/^{207}Pb$ versus $^{206}Pb/^{207}Pb$ plots (Figure 4). We interpret linear trends as binary mixing between distinct mantle source regions and assume they extrapolate linearly to source compositions [*Rudge et al*., 2013]. An important observation from this analysis is that most samples from the eastern GSC, and those found immediately west of the 91°W transform fault, plot on the same well-defined FLO-DGM binary mixing lines in Pb isotopic space as basalts from NE, central and western Galápagos. The Pb isotope data for central and NE Galápagos fall, which we refer to as Galápagos Reference Lines, and are defined by the following equations:

$$^{206}Pb/^{207}Pb = 0.99349 * {}^{208}Pb/^{207}Pb - 1.24372 \quad (r^2 = 0.986),$$

$$^{207}Pb/^{206}Pb = 0.77965 * {}^{208}Pb/^{206}Pb - 0.76488 \quad (r^2 = 0.988).$$

The majority of basalts from the western GSC, Pinta and northwest Galápagos have elevated ^{208}Pb and in Figure 4 fall to the right of the Galápagos Reference Lines and toward the WD (recycled sediment) component of *Harpp and White* [2001]. The few samples from the eastern GSC that have elevated ^{208}Pb occur immediately east of the axial high between 89.2°W and 89.6°W. Surprisingly, this analysis indicates that the PLUME component is sparsely sampled in the northern and central Galapagos and the GSC. We conclude that melting of partially dehydrated, recycled ancient oceanic crust (FLO component) is occurring beneath central Galápagos and the eastern section of the ridge, which is closest to the present-day Galápagos plume stem.

3. "Deep" Lateral Transport of Mantle Volatiles Beneath a Rheological Boundary Layer

While western Galápagos basalts are notable for their primitive He and Ne isotopic ratios, noble gas isotopic anomalies are absent from GSC basalts (Figure 1) [*Graham et al*., 1993, 2014; *Kurz and Geist*, 1999; *Detrick et al*., 2002; *Kurz et al*., 2009; *Colin et al*., 2011]. It has been proposed that the absence of a plume signal in helium isotopes on the GSC is because He is highly incompatible and removed during deep incipient melting in the plume stem [*Kurz and Geist*, 1999; *Villagómez et al*., 2014]. H_2O is, however, less strongly incompatible and the spatial variability in H_2O contents of mantle melts both at the spreading center and in the archipelago provides important information on melting and transport mechanisms. H_2O contents have been analyzed in olivine-hosted melt inclusions from a few Galápagos islands in the Galapagos Archipelago (Fernandina and Santiago [*Koleszar et al*., 2009]) and also in basaltic glasses from the GSC [*Detrick et al*.,

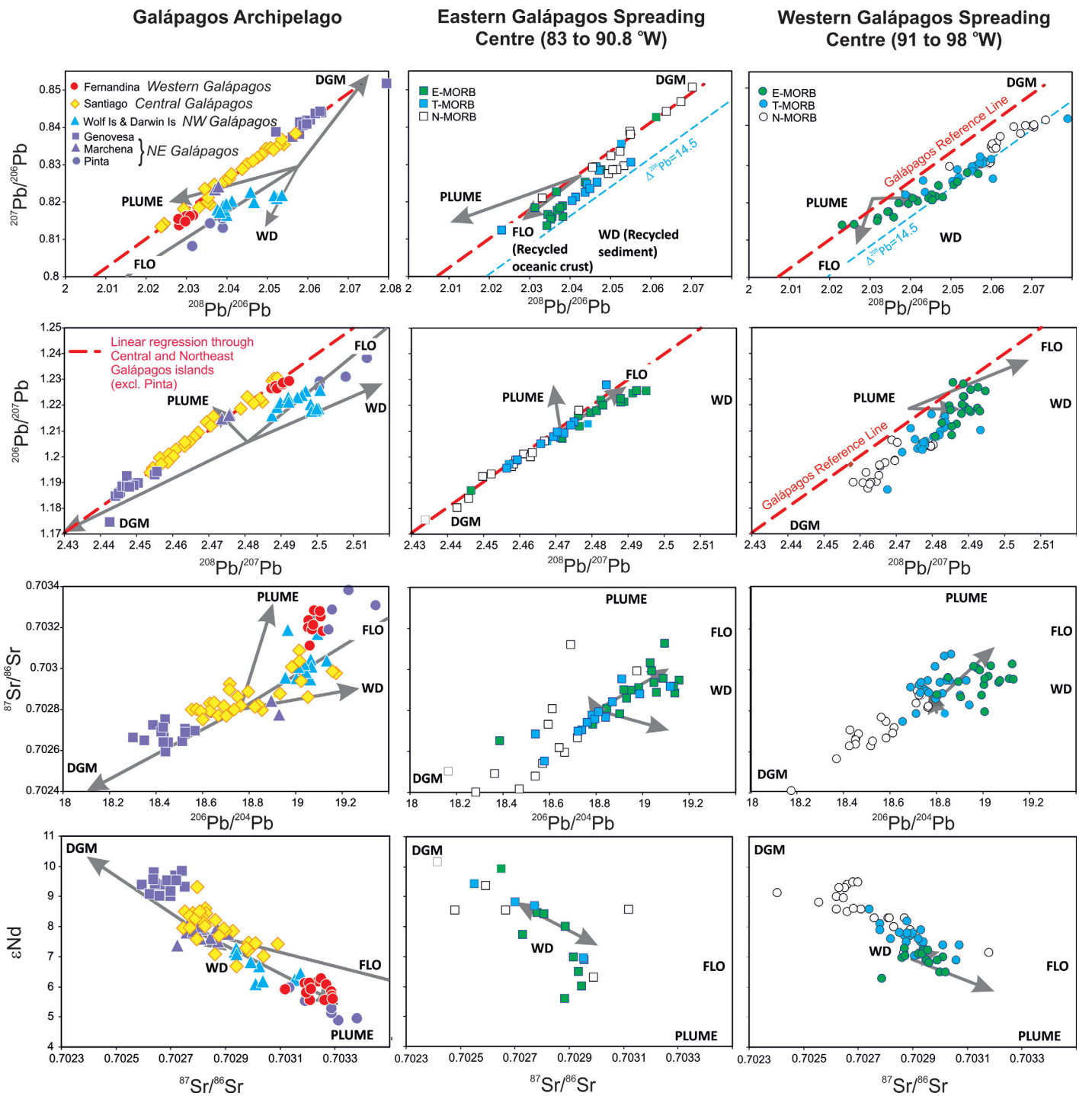

Figure 4. Variations in Sr, Nd, and Pb isotopic ratios in basalts from central and northeast Galápagos and the Galápagos Spreading Center. Gray vectors are derived from Principal Component Analysis (PCA) of Sr, Nd, and Pb isotopic ratios (supporting information Tables S1 and S2). PLUME, DGM, FLO, and WD are isotopically distinct reservoirs in the Galápagos plume [*Harpp and White*, 2001]. Our PCA analysis reveals that the PLUME component makes only a small contribution to GSC basalts and is consistent with *Schilling et al.* [2003]. Dashed blue line indicates the deviation in $^{208}Pb/^{206}$ ratios from the linear regression line for samples that fall on the Galápagos Reference Line (red dashed line) and is calculated using the following equation: $\Delta^{208}Pb = (^{208}Pb/^{206}Pb_{GRL} - {}^{208}Pb/^{206}Pb_{WGSC})*1000$. Analyses of Fernandina, Wolf, and Darwin Island basalts are shown for comparison. Data are from *White et al.* [1993], *Schilling et al.* [2003], *Saal et al.* [2007], *Ingle et al.* [2010], *Gibson et al.* [2012], and *Harpp et al.* [2014b].

2002; *Asimow and Langmuir*, 2003; *Cushman et al.*, 2004], and these analyses are useful in constraining mechanisms of dispersal of plume material, because H_2O exerts very strong controls on the depth of melting.

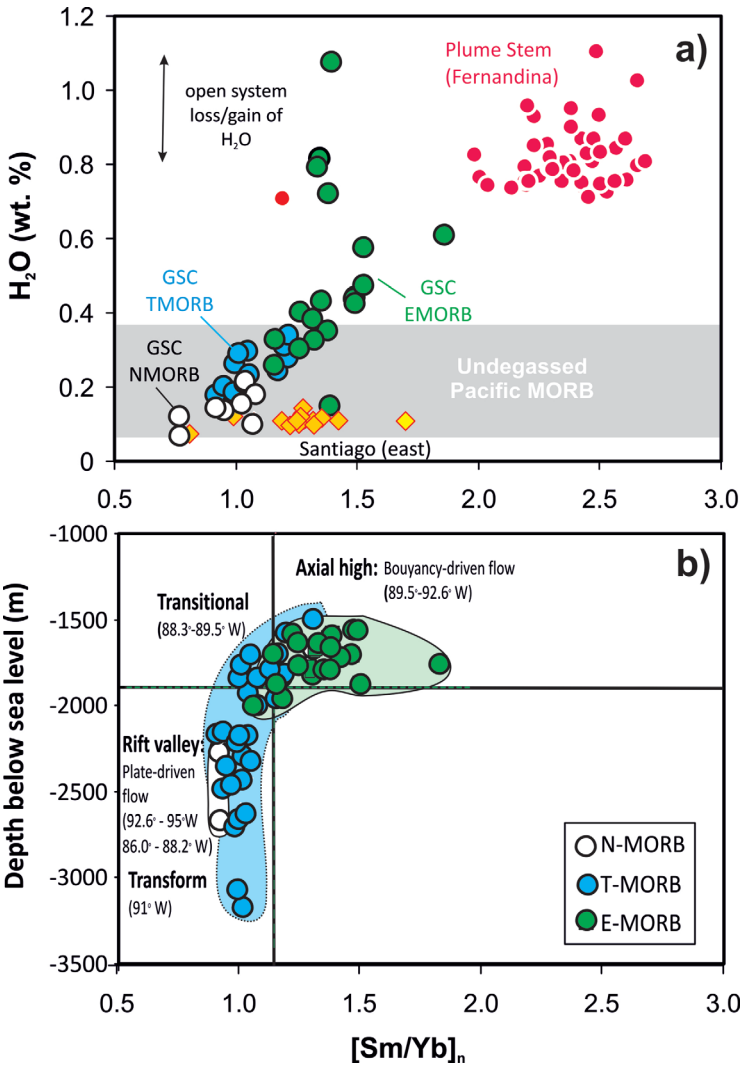

Figure 5. Variations in $[Sm/Yb]_n$ and H_2O of GSC basalts with bathymetry. (a) $[Sm/Yb]_n$ typically increases with H_2O contents in basaltic glasses from the western Galápagos Spreading Center (GSC) and also in olivine-hosted melt inclusions from the Galápagos archipelago. This reflects deep melting of volatile-rich mantle. The field for undegassed Pacific MORB (analyzed from melt inclusions from the Juan da Fuca Ridge) is shown for comparison. (b) $[Sm/Yb]_n$ decreases as the bathymetric height of the GSC increases and correlates with different styles of mantle flow through the melt column. Data are from *Schilling et al.* [1982], *Christie et al.* [2005], *Cushman et al.* [2004], *Detrick et al.* [2002], *Koleszar et al.* [2009], *Ingle et al.* [2010], and *Helo et al.* [2011]. Normalization factors are from *McDonough and Sun* [1995].

Investigations of basaltic glasses from the western GSC reveal that, in addition to elevated incompatible trace element, $^{206}Pb/^{204}Pb$, and $^{87}Sr/^{86}Sr$, and low $^{143}Nd/^{144}Nd$, E-MORB have higher H_2O contents than T-MORB and N-MORB [*Detrick et al.*, 2002; *Asimow and Langmuir*, 2003; *Cushman et al.*, 2004]. Figure 5 shows that there is a positive correlation between H_2O content and Sm/Yb, which we interpret as evidence of deep melting of volatile-bearing mantle between 92.5°W and 89.5°W. Moreover, olivine-hosted melt inclusions found in MORB-like low-K tholeiites from central Galápagos (eastern Santiago) have similar H_2O contents and $[Sm/Yb]_n$ ratios to GSC N-MORB [*Koleszar et al.*, 2009] (Figure 5a). Both H_2O contents and $[Sm/Yb]_n$ ratios are much lower in these basalts than in those from western Galápagos: melt inclusions from Fernandina basalts have the highest H_2O contents (Figure 5a) so far analyzed in Galápagos [*Koleszar et al.*, 2009]. The lower water concentrations of mantle melts in central Galápagos most likely correspond to: (i) relatively large amounts of upwelling and melting (15–20%) of depleted mantle beneath thin lithosphere (~45 km) [*Gibson and Geist*, 2010; *Villagómez et al.*, 2011; *Gibson et al.*, 2012] and (ii) removal of significant quantities of volatiles during plume-driven vertical upwelling and melting in the stem prior to lateral outward dispersal in the shallow mantle [*Kurz and Geist*, 1999; *Villagómez et al.*, 2014]. More H_2O and Pb isotopic data are

required for Galápagos and also the eastern GSC to establish if it is the PLUME and/or FLO mantle reservoir that is rich in H_2O.

The high H_2O concentrations of plume-influenced GSC MORBs [*Detrick et al*., 2002] indicate that material is reaching the ridge at depths greater than that of the anhydrous peridotite solidus and provide important constraints on the depth of dispersal of Galápagos plume material. While the effect of water on mantle rheology is under debate [cf. *Hirth and Kohlstedt*, 1996; *Fei et al*., 2013], here we follow the model of *Ito et al*. [1997] which proposes that a rheological boundary between hydrous and dehydrated peridotite forces most plume material to flow laterally at depths below the hydrous solidus. For Galápagos, the T_P of the plume is ~1400°C (supporting information Table S3), lateral flow of low-viscosity, volatile-bearing mantle will occur at depths >~80 km [*Gibson and Geist*, 2010]. Where localized upwelling of the overlying anhydrous peridotite occurs—such as beneath the thin lithosphere of central and northeast Galápagos—underlying hot, low-viscosity plume material will also passively decompress and may undergo partial melting. We suggest that melting away from the plume stem requires the coincidence of thin lithosphere, fertile mantle, and high temperatures, which is why the northern Galápagos volcanoes exist and Galápagos volcanism is more widespread than in other archipelagos.

Isotopically depleted basalts from central and northeast Galápagos (e.g., eastern Santiago and Genovesa) were generated <200 km from the center of plume-driven mantle upwelling (Figure 1) and, as we have shown above, contain smaller proportions of melts from the PLUME source and recycled ancient oceanic crust (FLO mantle) than more distal E-MORB on the adjacent GSC (Figures 2 and 4). That the GSC erupts more enriched basalts than does the northern Galapagos implies that ridgeward dispersal of plume material is more complex than current conceptual geodynamic models, which invoke radial gravitational flow and progressive dilution of plume material. In the gravitational flow regime, there is a "puddle" of plume material of lateral dimension comparable to the distance along the ridge in which enriched geochemical signatures are seen (~970 km for the GSC [*Feighner and Richards*, 1995]). Radial flow along the base of the lithosphere is not easily reconciled with the relatively depleted isotopic signatures of recently erupted basalts from the central and northern Islands and the absence of seamounts to the west of the Wolf-Darwin lineament (Figure 1).

The isotopic ratios of GSC basalts are to a large extent decoupled from incompatible trace element ratios (Figure 3), which suggests that the compositions and volumes of the erupted melts are influenced by both chemical heterogeneity in mantle source regions and melting processes. Both Galápagos plume-driven "deep" volatile-rich melting and plate-limited "shallow" anhydrous melting have been suggested as important processes in the formation of magma on the GSC west of the 91°W transform fault [*Cushman et al*., 2004; *Ingle et al*., 2010]. A first-order observation from our study is that the geochemical signatures of GSC E-MORB, both west and east of the 91°W transform fault, are due to the increased contribution of deep melts derived from partially dehydrated, recycled ancient oceanic crust (FLO mantle). Homogenization of these melts, and their channelized ascent in relative isolation from shallower melts, would preserve their geochemical signatures [*Katz and Weatherley*, 2012] in GSC basalts. We have shown above that deep melting of recycled oceanic crust extends into the garnet stability field, which is why aggregate melts have high Sm/Yb and low La/Nb ratios, and are isotopically enriched, relative to GSC melts resulting from plate-driven flow and melting of less fertile mantle at shallower depths (Figure 2).

4. Spatial Variations of V_s and Temperature in the Galápagos Mantle

The variations in incompatible trace element and isotopic ratios of basalts from the Galápagos Archipelago and adjacent spreading center that we have described above place independent constraints on interpretations of geophysical investigations of the region. The seismic models of *Villagómez et al*. [2007, 2014] show large spatial variations in V_S in the sub-Galápagos mantle (Figure 6a), and depth slices between 50 and 110 km exhibit a low-velocity anomaly extending beneath northeast Galápagos and the GSC. While this anomaly occurs where there are few crossing seismic rays, we note that it correlates almost exactly with our proposed region of ridgeward flow of plume material based on geochemistry and ridge morphology (see below).

Variations in V_S of the magnitude found in the study by *Villagómez et al*. [2007] are thought to be predominantly controlled by temperature and—to a lesser extent—differences in composition, grain size, and water

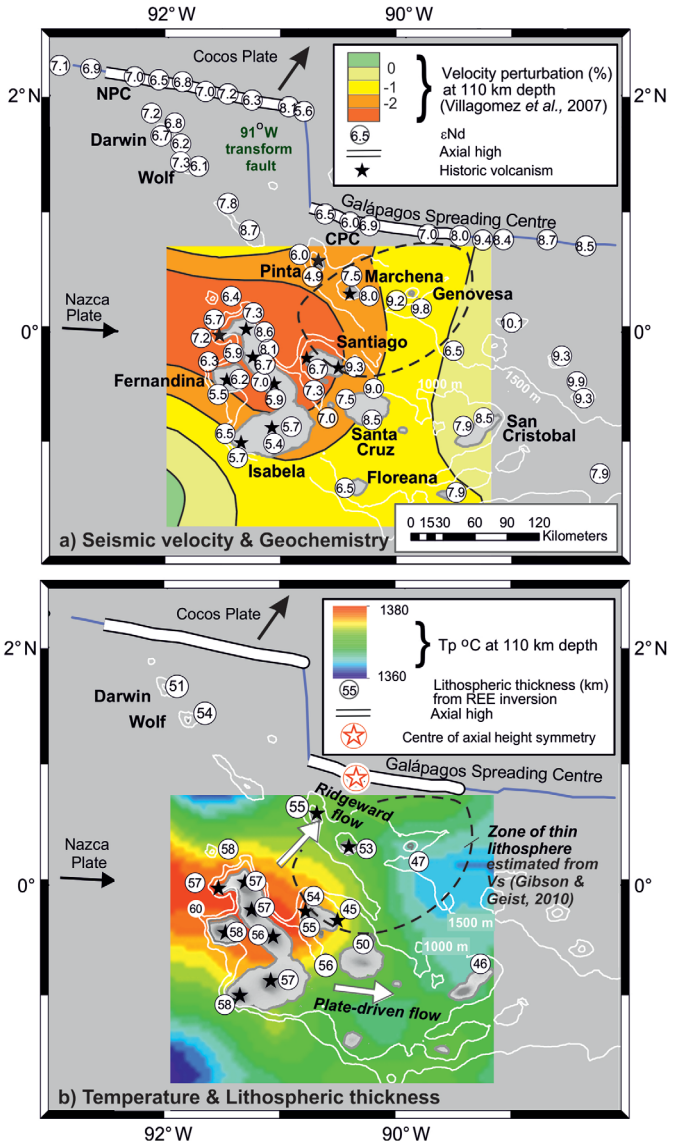

Figure 6. Variations in (a) seismic velocity at 110 km depth and εNd and (b) mantle potential temperature at 110 km depth and lithospheric thickness. Seismic data are from *Villagómez et al.* [2007], and temperatures were calculated using the parameterization of *Priestley and McKenzie* [2006], which is based on seismic data for the Pacific Ocean [see *Gibson and Geist*, 2010]. The estimated temperature at a given pressure was converted to T_P assuming a mantle adiabat of 0.6°C km. The temperature map was generated using a normal kriging algorithm. Estimates of lithospheric thickness, from REE inversion of the whole-rock compositions of recently erupted basalts, exclude older eruptions on Santa Cruz and San Cristobal [*Gibson and Geist*, 2010]. Similar lithospheric thicknesses have been calculated from seismic data and also correspond with thickness estimates based on the age of the underlying plate [*Gibson and Geist*, 2010; *Villagómez et al.*, 2011]. Note that the expected first-order thinning of the lithosphere toward the ridge does not apply for Galápagos. Bathymetric contours are from http://www.pmel.noaa.gov/vents/staff/chadwick/ Galápagos.html. Open star in circle at 90.42°W represents the center of symmetry of the isostatic axial depth profile [*Ito et al.*, 1997]. Note how the axial high corresponds to the predicted intersection of warm plume mantle with the GSC. The temperature difference along the ridge is similar to that proposed by *Ito et al.* [1997] and *Asimow and Langmuir* [2003]. CPC and NPC are the Central and Northern Plume Components identified by *Kokfelt et al.* [2005]. Geochemical data are from *Schilling et al.* [1982], *White et al.* [1993], *Geist et al.* [1995], *Naumann and Geist* [1999], *Harpp and White* [2001], *Detrick et al.* [2002], *Cushman et al.* [2004], *Christie et al.* [2005], *Saal et al.* [2007], *Ingle et al.* [2010], and *Gibson and Geist* [2010]. Normalization factors are from *McDonough and Sun* [1995]. Vectors of plate motions are from *Gripp and Gordon* [2002].

concentration caused by partial melting, and/or the amount of melt present [*Faul and Jackson*, 2005; *McKenzie et al.*, 2005; *Schutt and Lesher*, 2006; *Goes et al.*, 2012]. An empirical relationship between V_S, temperature, and pressure for Pacific Ocean lithosphere was established by *Priestley and McKenzie* [2006] who showed that there is a rapid, nonlinear decrease in V_S at temperatures close to the anhydrous peridotite solidus. The parameterization of *Priestley and McKenzie* [2006] is thought to be most appropriate for regions of young oceanic lithosphere and where potential mantle temperature is ambient (i.e., 1315°C) or has a moderate excess (<100°C) [*Schutt and Dueker*, 2008]. Here we assume that the effect of temperature is dominant and have examined spatial variations in V_S at depths below that of the anhydrous peridotite solidus (90–120 km).

4.1. Radial Spreading of a Plume "Puddle" Versus Channelized Plume Outflow

The lateral variation in temperature of the Galápagos plume is believed to be very small (<50°C) [*Villagmez et al.*, 2007]. At a depth of 110 km, the lowest V_S and hence highest estimated temperatures occur beneath western Galápagos (Figure 6). This spatially large anomaly (130 km × >170 km) coincides with the area of most active volcanism and the most primitive noble gas isotopic compositions and is therefore interpreted to be the stem of the Galápagos plume [*White et al.*, 1993; *Kurz and Geist*, 1999; *Villagmez et al.*, 2007, 2014]. Seismic velocities [*Villagómez et al.*, 2014] indicate that outflowing plume material is being dispersed asymmetrically rather than retaining the radial symmetry predicted by some conceptual models for ridge-centered plumes [cf. *Ribe and Delattre*, 1998; *Shorttle et al.*, 2010].

We interpret the seismically slow region between 100 and 120 km as being relatively hot Galápagos plume material flowing northeast toward the nearest section of the GSC. The elongation of this seismic anomaly is parallel to: (i) a zone of thin lithosphere beneath NE Galápagos [*Gibson and Geist*, 2010], (ii) the present-day NE azimuth of Cocos Plate motion [*Gripp and Gordon*, 2002; *Argus et al*., 2011], and (iii) the direction in which the GSC is migrating away from the plume [*Wilson and Hey*, 1995]. While the limited aperture and resolution of V_S variations in northern Galápagos and the corresponding inferred temperature anomalies are reason for caution in interpreting the dimensions of the deep zone of flow, we note that north-easterly flow of plume material coincides with historic volcanism on the islands of Pinta and Marchena and recent activity at Genovesa [*Harpp et al*., 2014a]. There appears to be no marked decrease in seismic velocities (and interpreted T_P) of plume material as it is dispersed from the zone of buoyant upwelling beneath western volcanoes toward the GSC (Figure 6b). The ~55°C difference in temperature between the GSC and ambient mantle, and the ~10°C variation that we estimate between 91°W and 88°W on the eastern GSC concurs with findings that apply other methods to estimate T_P (supporting information Table S3) [*Feighner et al*., 1995; *Ito and Lin*, 1995a; *Canales et al*., 2002; *Asimow and Langmuir*, 2003; *Cushman et al*., 2004].

Many enriched basalts (defined by elevated $^{208}Pb/^{204}Pb$) in NW Galápagos and from the western and eastern GSC reside outside the postulated zone of high-temperature plume flow (Figure 6). We propose that a second zone of high ^{208}Pb material flows more directly north, creating the axial high on the western GSC, the Wolf-Darwin Lineament and the numerous seamounts in the inside corner of the 91° transform. There is no seismic coverage in this part of Galápagos (Figure 6) [*Villagómez et al*., 2007], however, this hypothesis is consistent with *Kokfelt et al*. [2005], who suggest two isotopically distinct regions of plume material are flowing toward the GSC: one northwest beneath Wolf and Darwin Islands and another northeast, exactly in the region we have identified in this study.

4.2. The Role of the Thermal Lithosphere in Galápagos Plume-Ridge Interaction

Previous studies of plume-ridge interactions have highlighted the importance of thermal erosion in carving a lithospheric channel to the adjacent spreading center [*Morgan*, 1978; *Schilling et al*., 1985; *Schilling*, 1991; *Kincaid et al*., 1995; *Kingsley and Schilling*, 1998; *Sleep*, 2002]. Seismic and petrologic estimates (Figure 6b) indicate that the lithosphere is thinner by ~10 km in the area that extends to the NE of the archipelago toward the ridge. This is too small, however, compared to the thickness of the plume material (~70 km beneath the ridge [*Feighner and Richards*, 1995]) to trap plume material and influence outflow paths.

5. Correlating Geochemical and Geophysical Anomalies on the Galápagos Spreading Center

Along the 970 km zone of the GSC that is influenced by the Galápagos plume both geochemical and geophysical data exhibit long wavelength variations [*Schilling et al*., 1982, 2003; *Ito and Lin*, 1995b; *Ito et al*., 1997; *Ingle et al*., 2010; *Graham et al*., 2014]. *Schilling et al*. [2003] and *Christie et al*. [2005] showed that an eastern geochemical peak is defined by elevated $^{206}Pb/^{204}Pb$ together with low $^{143}Nd/^{144}Nd$ and $^{176}Hf/^{177}Hf$ isotopic ratios and occurs between 90.58°W and 91°W, and roughly coincides with the peak in geophysical data. They likewise show that a western geochemical peak is best defined by elevated $^{87}Sr/^{86}Sr$, $^{207}Pb/^{204}Pb$, and $^{208}Pb/^{204}Pb$ ratios and is located between 91.67°W and 92.17°W, slightly east of the intersection of the GSC and Wolf Darwin lineament (Figure 7). Additionally, when basalts from the 91°W transform are excluded (the intratransform lavas have anomalous compositions), MORB erupted between 90°W and 92.17°W has elevated $[La/Sm]_n$ and $[Sm/Yb]_n$. Figure 7 shows that if the low V_S anomaly of *Villagmez et al*. [2007] is extrapolated ~50 km NE (89.5°W–91°W), it coincides with (i) the major axial high on the eastern GSC; (ii) greatest crustal thickness (~10 km); and (iii) the eastern isotopic peak [*Schilling et al*., 1982, 2003; *Ito et al*., 1997, 2003; *Canales et al*., 2002; *Detrick et al*., 2002; *Sinton*, 2003; *Cushman et al*., 2004; *Christie et al*., 2005; *Kokfelt et al*., 2005; *Ingle et al*., 2010; *Mittelstaedt et al*., 2014].

Both *Christie et al*. [2005] and *Kokfelt et al*. [2005] recognize that the eastern and western geochemical peaks on the GSC represent locations of melting of different Galápagos plume components beneath the ridge. While findings from our study concur with this interpretation an important advance is that we link the enriched plume component associated with the eastern geochemical peak is related to melting of partially dehydrated, ancient recycled oceanic crust (i.e., the FLO mantle reservoir). The smaller concentrations of incompatible trace elements, and low Ba/Nb, La/Sm, and Nb/Zr, in E-MORB from the eastern GSC combined

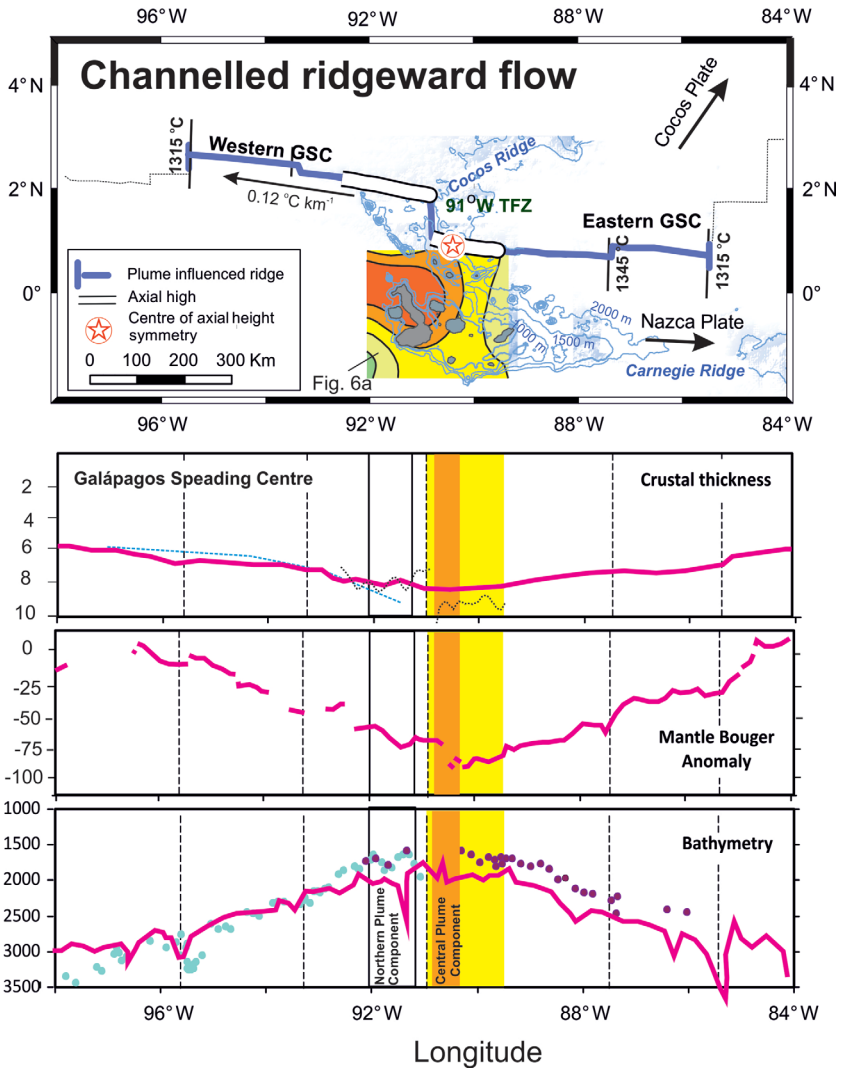

Figure 7. (a) Comparison of variations of mantle potential temperature at 110 km depth (from Figure 6b) with profiles of crustal thickness, mantle Bouger anomalies, and bathymetry for the Galápagos Spreading Center (GSC). Estimates of crustal thickness are from *Ito and Lin* [1995b] (red solid line), *Canales et al.* [2002] (blue dashed line), and *Mittelstaedt et al.* [2014] (black dotted line). Mantle Bouger anomalies are from *Ito et al.* [1997]. Axial depths are from *Ingle et al.* [2010] (closed blue circles) and *Christie et al.* [2005] (closed red circles) and are sampling depths. Bathymetric profile (red line) is corrected for crustal thickness and from *Ito et al.* [1997]. Locations of the Central and Northern Plume Components are from *Kokfelt et al.* [2005]. Vectors of plate motions are from *Gripp and Gordon* [2002]. (b) Variations in elemental and isotopic ratios with longitude on the GSC. Data are from *Schilling et al.* [1982], *Byers et al.* [1983], *Detrick et al.* [2002], *Schilling et al.* [2003], *Cushman et al.* [2004], *Christie et al.* [2005], and *Ingle et al.* [2010]. $\Delta^{208}Pb = ({}^{208}Pb/{}^{206}Pb_{GRL} - {}^{208}Pb/{}^{206}Pb_{WGSC})*1000$ (see caption of Figure 4). V_S variations beneath the Galápagos archipelago 110 km depth are from Figure 6a. Amounts of FLO (Floreana) and DGM (depleted Galápagos mantle) are shown as PC scores (see Table S2).

with higher ridge elevation (~1 km) [*Mittelstaedt et al.*, 2012] relative to the western GSC indicate larger amounts of adiabatic decompression melting or melting of this more fertile mantle: partially dehydrated, recycled oceanic crust will be more readily fusible and melt at higher pressures than the surrounding peridotite. We propose that greater melt productivity associated with the eastern GSC axial high partly reflects the presence of slightly higher-temperature, lower-viscosity, more buoyant plume mantle entering the base of the melt column at the ridge axis.

Gradients in isotopic and some of the elemental characteristics of GSC basalts are unaffected by ridge offsets (Figure 7b), which suggests that they were established in the dispersed plume material before it reached the ridge [*Schilling et al.*, 2003]. Moreover, the geochemical enrichments and similarity in compositions of E-MORB, erupted immediately west of the 91°W transform fault, to basalts in central and NE

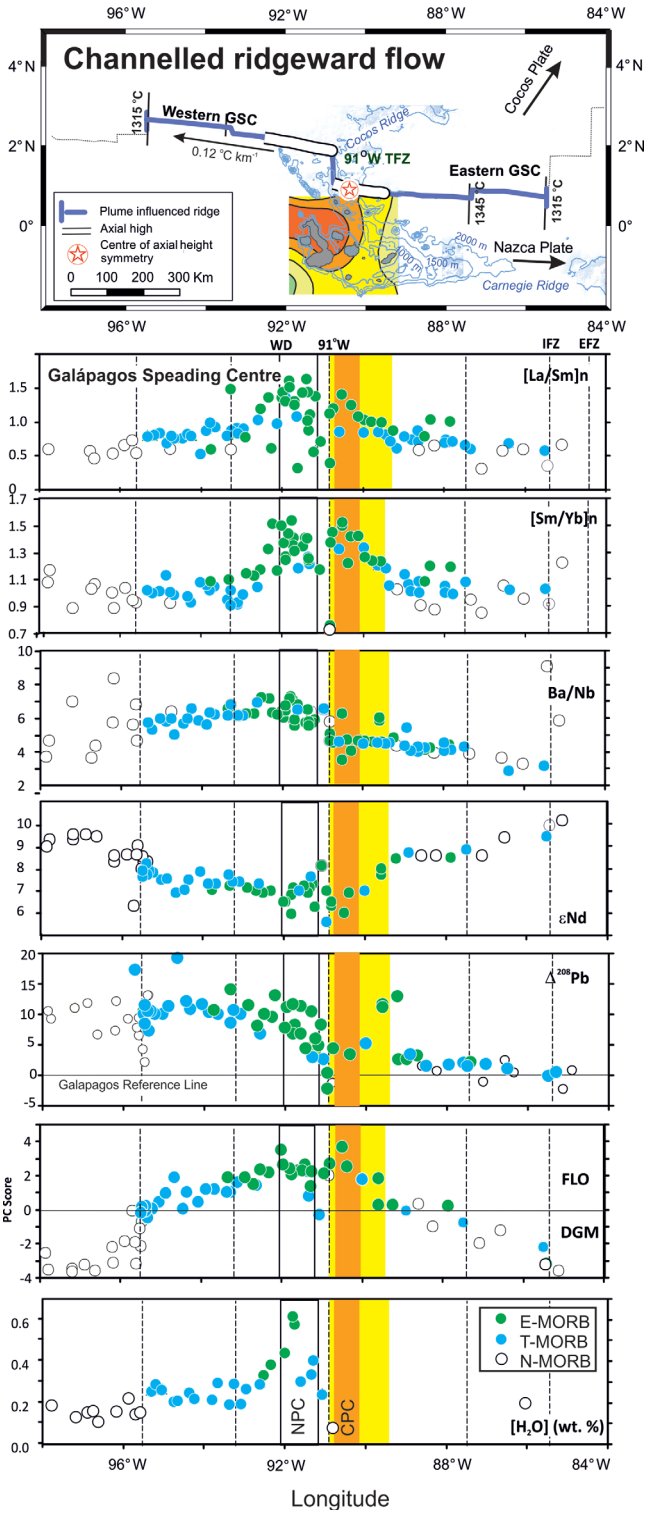

Figure 7. (continued)

Galápagos (Figures 2 and 4) imply they are tapping the same melt source region(s) in the underlying mantle. We suggest this may relate to deep plume material being dragged westward, perhaps following subridge flow lines inherited from when the plume was centered beneath the GSC between ~12 and 5 Ma (see below). Such a scenario would explain the low $^{3}He/^{4}He$ of basalts on the western GSC (Figure 1).

6. Constraints on the Geometry and Kinematics of Galápagos Plume-Ridge Interaction

6.1. Variable Rates of Plume Upwelling

Our geochemical and geophysical observations of the Galápagos plume-ridge system require a model that involves a narrow zone of flow of highest temperature, compositionally heterogeneous mantle from the plume stem to the nearest section of the GSC at depths below the anhydrous peridotite solidus (>80 km). Regional variations in Galápagos plume temperature are calculated to be small [*Villagómez et al.*, 2007] and do not fully explain the large spatial variations in compositions of erupted melts (Figure 6b) [cf. *White et al.*, 1993]. Numerical models of plume-driven flow predict that upwelling rates will be greater near the base of the melting region, such that the compositions of aggregate fractional melts are more heavily weighted toward those of deep incremental melts than in models of uniform upwelling [*Ito and Mahoney*, 2005; *Ito et al.*, 1999, 1997; *Maclennan et al.*, 2001]. In the zone separating the plume stem from the nearest section of ridge, U-series data are limited but suggest mantle upwelling is slow (2 cm yr^{-1}) [*Saal et al.*, 2000] relative to plate motion and we infer from this that north-easterly plume outflow beneath central and NE Galápagos is essentially lateral and the relative contribution of deep enriched melts to the final melt aggregate is small compared to at the plume stem and EGSC. The depleted nature of melts generated in the region between the plume stem and nearest section of ridge (e.g., eastern Santiago and Genovesa) may also reflect the trajectory of mantle material: some may have undergone melting during upwelling at

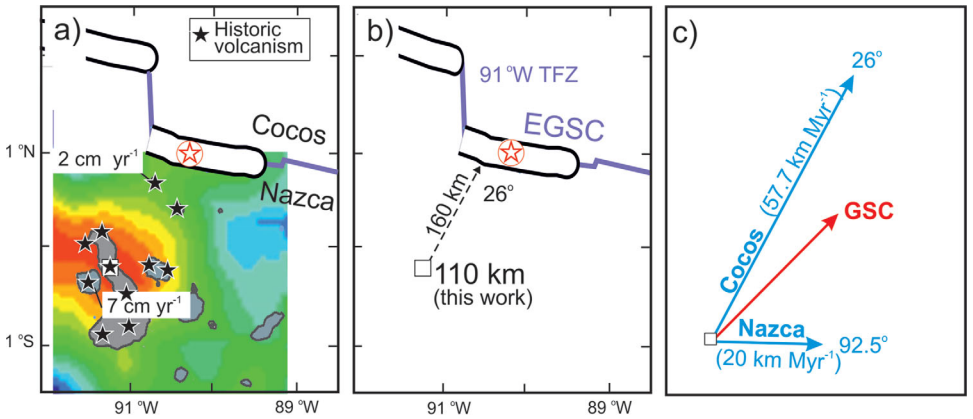

Figure 8. Schematic illustrations of relationships between mantle flow and plate motions beneath Galápagos. (a) V_S variation beneath Galápagos at 110 km depth (from Figure 6a) together with upwelling velocities from *Saal et al*. [2000]. (b) The relationship between the center of the plume upwelling (open squares) at a depth of 110 km and the center of axial height symmetry (open star) on the Galápagos Spreading Center (GSC). (c) The azimuth of confined plume stem-to-ridge flow is the same as the motion of the Cocos Plate. Estimates of plate motions are from the HS3-NUVEL_1A data set of *Gripp and Gordon* [2002].

the stem of the plume, prior to lateral flow toward the ridge as proposed by *Hoernle et al*. [2000] and illustrated in Figure 6.

6.2. Ridge "Capture" and "Anchoring" of Material Upwelling in the Galápagos Plume Stem

The Galápagos plume was ridge-centered between 12 and 5 Ma [*Wilson and Hey*, 1995; *Werner*, 2003; *Harpp et al*., 2005] and subsequent migration of the Galápagos Spreading Center (GSC) ~160 km to the northeast has been associated with numerous ridge jumps and development of transform faults [*Mittelstaedt et al*., 2012]. The most prominent transform fault, at ~91°W, displaced the eastern GSC south of the western GSC in two phases during the last 3 Ma [*Mittelstaedt et al*., 2012] (Figure 1), and has resulted in the separation distance between the current center of the shallow plume stem and the adjacent spreading center ranging from 160 km east of the 91°W transform fault to 250 km west of this structure.

We propose that confined, northeasterly oriented, deep ridgeward flow of compositionally and lithologically heterogeneous plume material has arisen because, following ridge capture between 12 and 5 Ma, material upwelling in the stem of the Galápagos plume has been "anchored" to the ridge (primarily to the east of 91°W). As the ridge migrated away from the plume, a broad (~175 km wide) channel of relatively high-temperature plume flow has developed. This anchoring of material flowing from the plume stem to a contact point on the GSC is determined by the buoyancy flux and temperature (viscosity) of the plume together with the rate of NE migration of the GSC (Figure 9). The channel of relatively high-temperature (and low viscosity) NE ridgeward flow occurs at depths >100 km and is embedded within the normal spreading and advection of Galápagos plume material, and intersects the eastern GSC where the axial bathymetric height is greatest. Figure 8 shows that the channel has the same NE azimuth as the motion of the Cocos Plate [*Gripp and Gordon*, 2002]. Moreover, we propose that the location of the major 91°W transform fault may have been influenced by tensional lithospheric stresses associated with plate motions, anchoring of the plume stem to the eastern GSC, and confined high-temperature plume outflow. We further suggest episodic stress release may have controlled the two phases of southward movement on the 91°W transform fault that have resulted in a nearly fixed plume-ridge separation distance of 145–215 km during the last 3 Ma [*Mittelstaedt et al*., 2012].

6.3. Some Remarks on Possible Channeling of Plume Flow Toward the Ridge

In the foregoing sections, we have inferred that plume material is being dispersed toward the Galápagos Spreading Center at depths below the anhydrous peridotite solidus, likely through a channel dating from the last time the plume was ridge centered at ~5 Ma. A variety of geochemical, geophysical, and tectonic information supports this view, especially the evidence from GSC basaltic glasses that they contain deep, hydrous melts of enriched plume material (Figure 5). By contrast, we have shown above that relatively anhydrous, depleted material is melting beneath the NE and central Galápagos, and this material must therefore overlie the enriched plume material that is flowing ridgeward from the deep mantle plume. Two distinct

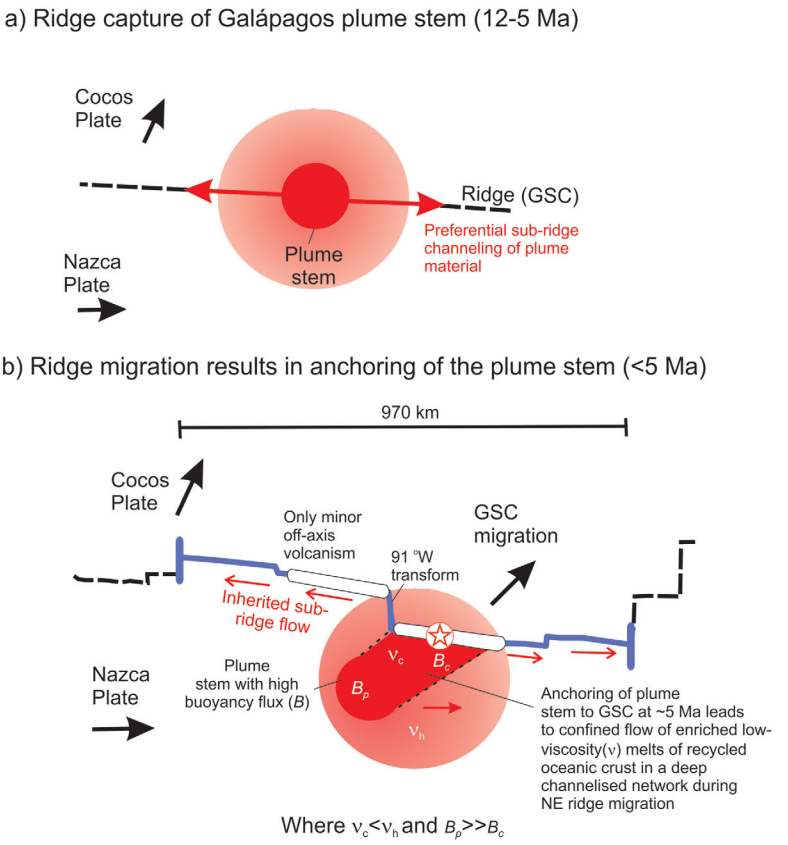

Figure 9. Temporal evolution of Galápagos plume-ridge flow. Observed variations in compositions of melts generated between the Galápagos plume and ridge require a more dynamically complex model than simple radial outflow in a "puddle" of plume material. Large length-scale variations in ridge topography and melt thickness, combined with the lack of seamounts in regions between the plume and ridge to the west of ~92°W, are best explained by subridge flow of plume material rather than simple radial flow from the plume stem [cf. *Shorttle et al*., 2010]. The region of high temperature confined flow in Figure 9b correlates with the region of elevated crustal thickness (10 km) [*Mittelstaedt et al*., 2014] beneath the eastern GSC. We propose the zone of confined plume stem-to-ridge flow has been maintained since the plume was last ridge centered 12–5 Ma [*Wilson and Hey*, 1995; *Werner*, 2003; *Harpp et al*., 2005]. In this scenario, the location of confined plume stem-to-ridge flow may have influenced formation of the 91°W transform fault, which developed in two stages ~3 and 1 Ma [*Mittelstaedt et al*., 2012]. The location of the Galápagos plume stem at >200 km depth is from *Villagómez et al*. [2014].

fluid mechanical effects may be at play in generating the deep ridgeward flow, viscous fingering or return flow to the ridge, and may involve melt rather than solid-state transport.

6.3.1. Viscous Fingering Between the Galápagos Plume and Adjacent Spreading Ridge

Heat flow from a hot plume channel in the base of the lithosphere must be comparable to that out of the young overlying oceanic lithosphere in order for channelization to occur, and connecting the plume and ridge via a channel "burned" into the base of the lithosphere is under most circumstances unlikely [*Sleep*, 2008]. Another necessary condition is that a viscosity contrast of order at least ~30–100 between the plume channel material and the surrounding asthenosphere is required for a "fingering" instability to occur [e.g., *Helfrich*, 1995; *Wylie and Lister*, 1995]. Such a large contrast is certainly possible for the excess temperatures associated with the Galápagos plume (T_P = ~1400°C; Table S3), especially if a small degree of partial melting is present, as we have shown above appears likely at subanhydrous peridotite solidus depths.

6.3.2. Return Flow to the Ridge Confined Within the Upper ~200 km of the Mantle

Another fluid mechanical effect, which appears not to have been accounted for in previous geodynamic models for plume-ridge interaction, is that of confinement of return flow to the spreading ridge within a thin asthenospheric channel of very low viscosity. Many mantle dynamics models include a low viscosity

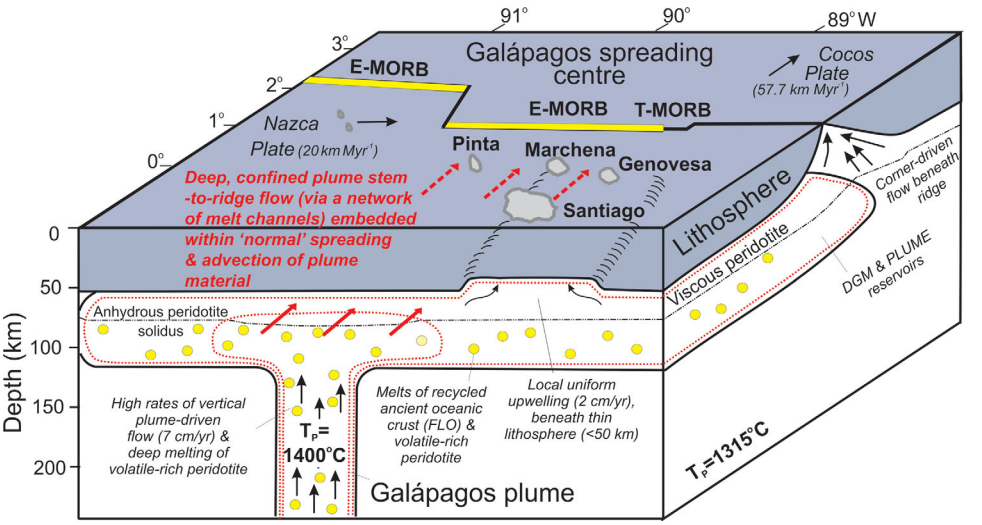

Figure 10. Conceptual model illustrating deep dispersal of Galápagos plume material via a "deep" network of melt channels to the adjacent spreading ridge (see text for detailed discussion). Note (i) the coincidence of the intersection of the region of confined flow of high-temperature plume mantle (red arrows) with the location of E-MORB on the eastern GSC and also (ii) the offset between the channel of ridgeward plume flow and the region of thin lithosphere. Filled circles represent "blebs" of fusible FLO mantle (partially dehydrated, recycled ancient oceanic crust) [*Harpp et al*., 2014a] at depths below the subanhydrous peridotite solidus. The overall contribution of the FLO reservoir to the isotopic signature of basalts in central and northeast Galápagos and on the GSC is small [*Harpp and White*, 2001].

upper mantle, "LVZ" or "asthenosphere," but they generally model the asthenosphere as filling the upper 400–670 km of the mantle (corresponding to prominent mantle phase transitions), and assume only modest viscosity contrasts of order ~3–100. However, all lines of evidence of which we are aware (including post-glacial rebound, the geoid, rotational dynamics, intraplate stresses, postseismic relaxation, and seismic anisotropy) are equally consistent with a very thin low-viscosity channel bottoming at ~200 km depth and representing a viscosity contrast of order at least ~1000 beneath the oceanic lithosphere [*Thoraval and Richards*, 1997; *Paulson and Richards*, 2009; M. A. Richards and A. Lenardic, manuscript in preparation, 2015]. The fundamental reason for this ambiguity is that the viscosity contrast required to satisfy most geodynamic constraints on upper mantle viscosity structure scales inversely with the cube of the channel thickness [*Cathles*, 1975; *Lenardic et al*., 2006; *Paulson and Richards*, 2009]. Thus, for example, a 300 km thick channel between the bottom of the lithosphere and the 400 km discontinuity that is a factor of 30 lower viscosity than that of the underlying mantle is essentially indistinguishable from a 100 km thick channel of viscosity contrast 810 (30×3^3) when modeling most data sets.

Of relevance to the present study, such a thin and very weak LVZ, or asthenosphere, effectively confines the return flow to a mid-ocean ridge within the asthenosphere itself [*Richards*, 1991]. Therefore, it is a reasonable hypothesis—especially in the vicinity of the ridge itself—that hot, buoyant mantle plume material will be strongly advected horizontally within the lower part of the asthenosphere toward the ridge, where it would undergo "deep," hydrous partial melting, as illustrated by the red arrows in Figure 10. The depleted melt residuum would then be advected horizontally away from the ridge immediately beneath the plate (beneath the NE and central Galápagos). This latter return flow confinement effect would be enhanced in a positive feedback sense if a low-viscosity channel had already been established between the ridge segment where the plume last impinged, as we have hypothesized in this paper. Unfortunately, this confluence of conditions—a thin, strong asthenosphere, overlying divergent plate motions, and a buoyant, off-ridge-axis plume—have not been incorporated together into geodynamic models for plume-ridge interaction, mainly because such large viscosity contrasts (asthenosphere plus effects of hot plume temperature and partial melting) occurring over such small length scales presents extreme computational challenges. Therefore the inferences we have made for channelized plume flow toward the ridge within the asthenosphere provides impetus for a new class of plume-ridge interaction models that should incorporate return flow to the ridge confined by a thin, very low viscosity asthenospheric channel at 200–100 km depth. Key questions for such studies would include that of whether small-scale convection within the sub-Galápagos asthenosphere (for which there is no conspicuous evidence) might disrupt the hypothesized plume-ridge channel, and the

degree to which ridgeward advection of plume material (via plate-induced return flow) would promote the kind of channeling instabilities that were investigated by *Sleep* [2008] for the case of no overlying plate motions and no asthenosphere.

6.3.3. Plume-Ridge Transport: Via Solid-State Flow or Melt Veins and Channels?

The foregoing discussion has been in terms of solid-state mantle flow and transport, as most models of plume-ridge interaction have been developed in this context, including those most recently proposed for Galápagos. For example, *Kokfelt et al*. [2005] concluded that dispersal of Galápagos plume material occurs in the solid state. This inference is based on U-series data which suggest that melt transport times between the Galápagos plume and GSC must be less than ~35,000 years, whereas numerical models predict melt migration over this distance would take 165,000 years [*Braun and Sohn*, 2003]. Nevertheless, the parameters in the *Braun and Sohn* [2003] model are by no means certain and a significant range of transport times is possible. More importantly, the *Braun and Sohn* [2003] model refers to a pervasive 2-D (sheet-like) region of partially molten mantle through which melt migration would be occurring by shallow porous flow, at a more or less uniform rate, over a huge areal extent between the plume and the ridge (i.e., ~10,000 km^2). By conspicuous contrast, as we have described above all evidence is that ridgeward flow is deep. If such flow occurs it is likely in pipe-like channels confined both vertically and horizontally to perhaps as little as tens of meters to a few kilometers in both directions, but elongated by about 100 km along the plume-to-ridge direction (see below). Confinement of ridgeward melt transport to narrow channels would increase the local flow rate over that predicted by *Braun and Sohn* [2003] by a large factor and hence there would be no problem matching the constraint imposed by the U-series data of *Kokfelt et al*. [2005].

The most recent numerical simulations of Galápagos plume-ridge interaction involve solid-state transport of plume material consisting of veins of geochemically enriched material set in a depleted matrix [*Ito and Bianco*, 2014]. The two models described by *Ito and Bianco* [2014] involve melting of plume material with (i) low viscosity and no dependence on water content and (ii) high viscosity in the shallowest mantle with the dependence of water content. Neither of these models, however, satisfactorily reproduces the observed variations in melt flux: the anhydrous melting model predicts a melt volume that is much higher than estimated from bathymetric and gravity data [*Feighner and Richards*, 1994]. In contrast, the model involving deep melting of volatile-bearing mantle is significantly influenced by the increase in mantle viscosity associated with dehydration, which restricts the extent of buoyancy-driven mantle upwelling, so that the predicted melt flux is not only low immediately above the plume stem (i.e., western Galápagos) but is ~50% less than observed for the ridge. Moreover, this model requires melting over an area much broader than the Galápagos platform. The failure of solid-state transport models involving both gravitational flow of anhydrous material and deep, confined flow of volatile-bearing mantle beneath a rheological boundary layer of dehydrated mantle to satisfactorily explain observed covariations in the spatial extent of melting and melt flux associated with the Galápagos plume confirms the complexity of processes involved in plume-ridge interaction.

An attractive possibility that has received remarkably little attention in this literature is that melt transport *via* veins and channels (two-phase flow) may dominate the geochemical signatures of plume-ridge interaction and lead to a focused melt flux. Although detailed modeling is beyond the scope of this paper, a simple plausibility argument can be made that melt transport via veins and channels, at depths below the anhydrous peridotite solidus and embedded in the normal spreading and advection of plume material, might be the case for Galápagos. Small-fraction, volatile-rich, low-viscosity melts are readily mobilized from their source regions [*McKenzie*, 1989] and develop an interconnecting network of channels formed naturally by melt migration instability [e.g., *Weatherley and Katz*, 2012]: this channelization of melts is perhaps evidenced at larger length scales by trends such as the Wolf-Darwin Lineament (and other subparallel volcanic chains) and by short wavelength variations in incompatible and isotopic ratios of melts erupted along the GSC between 92.5°W and 89.5°W (Figure 1). We envision deep melt transport may be either in the porous flow regime (with locally high permeability), the "mush" regime (with wholesale transport of melt and crystals), or almost pure melt channels. Gravitational ridgeward flow of melts of recycled oceanic crust in deep channels would be enhanced by the slope of the rheological boundary layer. This varies from ~72 ± 5 km at the ridge to ~91 ± 8 km above the plume [*Byrnes et al*., 2015]. For the past ~5 Ma the GSC has maintained a distance of order ~150–250 km north of the Galápagos plume via a series of ridge jumps, no one of which appears to be larger than ~30–50 km [*Mittelstaedt et al*., 2012]. If we assume that asthenospheric melt transport beneath ridges is dominated by stable melt channels—via some type of reactive infiltration instability process and that for anhydrous mantle and at

ambient temperatures these exist at depths of <80 km [*Aharonov et al*., 1995; *Katz and Weatherley*, 2012]—then it is straightforward to envision how a confined network of channels might be maintained during migration of the ridge from the plume stem. This requires no single ridge jump to exceed the typical horizontal extent of the melt-channeling zone beneath mid-ocean ridges (~50–70 km), as appears to be the case in the Galápagos. Given the difficulty reconciling the standard solid-state plume-ridge mixing paradigm with the data presented in this paper (Figure 10) and in the models of *Ito and Bianco* [2014], the situation in the Galápagos clearly points toward the need to explore two-phase flow models in greater detail in future work.

6.4. Implications for Models of Galápagos Plume-Ridge Interaction

The ridgeward flow of high-temperature plume material at depths greater than the anhydrous peridotite solidus that we have proposed above presents a paradox and also a challenge to the current state of geodynamic modeling of plume-ridge interaction. The paradox is that if there is relatively confined plume-stem-to-ridge flow then it is not obvious how to explain the ~970 km width of the geophysical and geochemical signature of the "plume" along the GSC. One possibility is that there is dispersed outward flow, forming a puddle of plume material ~970 km wide at the base of the lithosphere. Such a feature is not apparent from the distribution of surface volcanism, or geophysical and geochemical data (on both sides of the ridge). Instead, our findings suggest there may be flow of "captured" plume material below the ridge, both westerly and easterly, away from the closest ridge segment (Figure 9) [*Sleep*, 2002]. The 91°W transform fault must exert a minimal effect on along-ridge plume dispersal and is consistent with (i) the proposition that Galápagos plume material has been transported along the GSC at times of superfast spreading of the East Pacific Rise [*Geldmacher et al*., 2013] and (ii) the lack of inflections in isotopic ratios along this part of the GSC [*Graham et al*., 2014]. While this interpretation contrasts with the findings of early analytical studies, which predicted that ridge offsets would dam plume flow [*Vogt and Johnson*, 1975; *Schilling et al*., 1982], more recent numerical studies suggest that this effect is only significant for transform faults with offsets >100 km, because at smaller offsets the difference in lithospheric thickness on either side of the fault is too small to dam the flow of plume material [*Braun and Sohn*, 2003; *Weatherley and Katz*, 2010; *Georgen*, 2014]. The cumulative offset of the 91°W transform is ~90 km and has resulted in the juxtaposition of lithosphere with a small difference in age (5 Ma) and thickness (~10 km). Moreover, our model assumes that along ridge flow was inherited while the Galápagos plume was ridge centered and prior to the formation of the 91°W transform fault. Since movement on the transform fault has involved a series of southward displacements (initially 60 km at 5 Ma followed by 30 km at 1 Ma [*Mittelstaedt et al*., 2012]), at any one time the effective length of this ridge offset has been relatively small and only responsible for minimal disruption of shallow subaxial plume flow. Another possibility is that along-ridge flow is much deeper than the lithosphere-asthenosphere boundary.

Ribe and Delattre [1998] treated the case of the fluid-mechanical interaction between an off-ridge plume and a migrating ridge, including ridge migration at oblique angles, similar to the case of the GSC and Galápagos plume. Their work [following *Feighner and Richards*, 1995; *Ribe*, 1996; *Ito et al*., 1997] assumes that plume buoyancy and plate-driven advection dominate the signature of the plume along the ridge axis, that is, the disturbance of a radially spreading sublithospheric "puddle" of mantle plume material by the flow induced by the ridge. In this context, the inferred direction of flow from the plume stem north-eastward toward the nearest GSC segment, more or less along the direction of both the north-easterly Cocos Plate relative motion and migration of the GSC (Figures 8b and 9), is just as expected. The work of *Ribe and Delattre* [1998] also suggests that the "slope" of the lithosphere, due to aging away from the ridge, is not likely to affect the flow regime to first order. As yet there are no geodynamic models that fully capture the kinematic situation summarized in Figure 10, especially the presence of both oblique ridge migration and ridge-segment offset, and, perhaps more importantly, the influence of a thin, low-viscosity asthenospheric channel, or low-viscosity zone (LVZ). Nor do we currently have models that satisfactorily account for the effects of temperature-dependent viscosity in perhaps focusing (narrowing) sublithospheric plume flow that we have shown above. In a word, existing models are inadequate to account for the rich set of observations constraining plume-ridge interaction in the Galápagos.

7. Conclusions

The spatial distribution in historic Galápagos volcanism, geochemical and geophysical observables in the archipelago and adjacent Galápagos Spreading Centre (GSC) cannot be readily explained by dispersal of plume material either radially in a "puddle" at the base of the lithosphere or a "pipeline" in a shallow

sub-lithospheric channel to the ridge [c.f. *Schilling et al.*, 1982; *Braun & Sohn*, 2003; *Sleep*, 2008; *Shorttle et al.*, 2010]. Our Principal Component Analysis of Sr-Nd-Pb isotopic ratios of Galápagos and GSC basalts shows that geochemical signatures of E-MORB on the section of ridge nearest the plume are a result of preferential deep melting of partially-dehydrated, recycled, ancient oceanic crust (Floreana component) intrinsic to the plume. This component is also evident – but to a lesser and more variable extent – in basalts erupted between the plume stem and ridge. We infer that the first order control on the location of historic volcanism and the greatest amount of melt generation beneath the ridge, is a ~175 km wide, NE trending confined channel of plume stem-to-ridge flow that exists at depths below the anhydrous-peridotite solidus (*i.e.* >80 km).

We propose a two-stage model for the development and sustainment of a long-term (>5 Ma), confined zone of deep NE plume flow that involves initial on-axis capture of the upwelling plume stem by the GSC, and subsequent anchoring of this to a contact point on the ridge during NE migration of the spreading axis. We suggest confined plume flow occurs via a deep network of melt channels embedded in the normal spreading and advection of material in the Galápagos plume rather than by solid state transport [*Kokfelt et al.*, 2005; *Ito and Bianco*, 2014]. The physical parameters and styles of mantle flow that we have defined for Galápagos are not well constrained for other well-known sites of plume-ridge interactions, such as Easter Island in the Pacific, the Azores, St Helena and Tristan in the mid-Atlantic, and Amsterdam in the Indian Ocean. In many of these cases the presence of a mantle plume is contested. Our findings permit realistic parameters and boundary conditions to be used in dynamical models of global plume-ridge interactions and therefore aid understanding of what drives the most currently active volcanism on the surface of the Earth.

Acknowledgments

We thank Galápagos National Park authorities and CDRS for permitting fieldwork in Galápagos. D. Villagomez and D. Toomey generously shared their extensive seismic data set for Galápagos, and D. McKenzie kindly provided help with temperature calculations. End-member compositions of Galápagos mantle reservoirs in Figure 4 were estimated from principal component analysis; data related to these calculations are available in the supporting information. We are grateful to Kaj Hoernle and two anonymous reviewers for their constructive comments on an earlier version of this manuscript. The research was funded by the University of Cambridge, Geological Society of London, NERC (RG57434), and NSF (EAR 0838461, EAR 0944229, and EAR-11452711).

References

Aharonov, E., J. A. Whitehead, P. B. Kelemen, and M. Spiegelman (1995), Channeling instability of upwelling melt in the mantle, *J. Geophys. Res.*, *100*(B10), 20,433–20,450, doi:10.1029/95JB01307.

Argus, D. F., R. G. Gordon, and C. DeMets (2011), Geologically current motion of 56 plates relative to the no-net-rotation reference frame, *Geochem. Geophys. Geosyst.*, *12*, Q11001, doi:10.1029/2011GC003751.

Asimow, P. D., and C. H. Langmuir (2003), The importance of water to oceanic mantle melting regimes, *Nature*, *421*(6925), 815–820.

Bercovici, D., and J. Lin (1996), A gravity current model of cooling mantle plume heads with temperature-dependent buoyancy and viscosity, *J. Geophys. Res.*, *101*(B2), 3291–3309, doi:10.1029/95JB03538.

Blichert-Toft, J., and W. M. White (2001), Hf isotope geochemistry of the Galápagos Islands, *Geochem. Geophys. Geosyst.*, *2*(9), 1043, doi:10.1029/2000GC000138.

Braun, M. G., and R. A. Sohn (2003), Melt migration in plume-ridge systems, *Earth Planet. Sci. Lett.*, *213*(3–4), 417–430.

Byers, C. D., D. W. Muenow, and M. O. Garcia (1983), Volatiles in basalts and andesites from the Galapagos spreading center, 85° to 86°W, *Geochim. Cosmochim. Acta*, *47*(9), 1551–1558, doi:10.1016/0016–7037(83)90181-3.

Byrnes, J. S., E. E. E. Hooft, D. R. Toomey, D. R. Villagómez, D. J. Geist and S. C. Solomon (2015), An upper-mantle seismic discontinuity beneath the Galápagos Archipelago and its implications for studies of the lithosphere-asthenosphere boundary, *Geochem. Geophys. Geosyst.*, doi:10.1002/2014GC005694, in press.

Canales, J. P., G. Ito, R. S. Detrick, and J. M. Sinton (2002), Crustal thickness along the western Galápagos spreading center and the compensation of the Galápagos hotspot swell, *Earth Planet. Sci. Lett.*, *203*(1), 311–327.

Cathles, L. M. (1975), *The Viscosity of the Earth's Mantle*, Princeton Univ. Press, Princeton, N. J.

Christie, D. M., R. Werner, F. Hauff, K. A. Hoernle and B. B. Hanan (2005), Morphological and geochemical variations along the eastern Galápagos spreading center, *Geochem. Geophys. Geosyst.*, *6*, Q01006, doi:10.1029/2004GC000714.

Colin, A., P. G. Burnard, D. W. Graham, and Y. Marrocchi (2011), Plume-ridge interaction along the Galápagos spreading center: Discerning between gas loss and source effects using neon isotopic compositions and ^{4}He-$^{40}Ar^{*}$-CO_2 relative abundances, *Geochim. Cosmochim. Acta*, *75*(4), 1145–1160, doi:10.1016/j.gca.2010.11.018.

Cushman, B., J. M. Sinton, G. Ito, and J. E. Dixon (2004), Glass compositions, plume-ridge interaction, and hydrous melting along the Galápagos spreading center, 90.5°W to 98°W, *Geochem. Geophys. Geosyst.*, *5*, Q08E17, doi:10.1029/2004GC000709.

DeMets, C., R. G. Gordon, D. F. Argus, and S. Stein (1994), Effect of recent revisions to the geomagnetic reversal time scale on estimates of current plate motions, *Geophys. Res. Lett.*, *21*(20), 2191–2194, doi:10.1029/94GL02118.

Detrick, R. S., J. M. Sinton, G. Ito, J. P. Canales, M. D. Behn, B. Cushman, J. E. Dixon, D. W. Graham, and J. J. Mahoney (2002), Correlated geophysical, geochemical and volcanological manifestations of plume-ridge interaction along the Galápagos spreading center, *Geochem. Geophys. Geosyst.*, *3*(10), 8501, doi:10.1029/2002GC000350.

Faul, U. H., and I. Jackson (2005), The seismological signature of temperature and grain size variations in the upper mantle, *Earth Planet. Sci. Lett.*, *234*(1–2), 119–134.

Fei, H., M. Wiedenbeck, D. Yamazaki, and T. Katsura (2013), Small effect of water on upper-mantle rheology based on silicon self-diffusion coefficients, *Nature*, *498*(7453), 213–215, doi:10.1038/nature12193.

Feighner, M. A., and M. A. Richards (1994), Lithospheric structure and compensation mechanisms of the Galápagos Archipelago, *J. Geophys. Res.*, *99*(B4), 6711–6729.

Feighner, M. A., and M. A. Richards (1995), The fluid dynamics of plume-ridge and plume-plate interactions: An experimental investigation, *Earth Planet. Sci. Lett.*, *129*(1–4), 171–182, doi:10.1016/0012-821X(94)00247-V.

Feighner, M. A., L. H. Kellogg, and B. J. Travis (1995), Numerical modeling of chemically buoyant mantle plumes at spreading ridges, *Geophys. Res. Lett.*, *22*(6), 715–718, doi:10.1029/95GL00311.

Fitton, J. G. (2007), The OIB paradox, *Geol. Soc. Am. Spec. Publ.*, *430*, 387–412.
Geist, D. J. (1992), An appraisal of melting processes and the Galápagos hotspot: Major- and trace-element evidence, *J. Volcanol. Geotherm. Res.*, *52*(1–3), 65–82.
Geist, D. J., W. M. White and A. R. McBirney (1988), Plume-asthenosphere mixing beneath the Galápagos archipelago, *Nature*, *333*(6174), 657–660.
Geist, D. J., K. A. Howard, and P. Larson (1995), The generation of oceanic rhyolites by crystal fractionation: the basalt-rhyolite association at Volcán Alcedo, Galápagos Archipelago, *J. Petrol.*, *36*(4), 965–982.
Geist, D. J., T. Naumann, and P. Larson (1998), Evolution of Galápagos magmas: Mantle and crustal fractionation without assimilation, *J. Petrol.*, *39*(5), 953–971.
Geist, D. J., T. R. Naumann, J. J. Standish, M. D. Kurz, K. S. Harpp, W. M. White, and D. J. Fornari (2005), Wolf Volcano, Galápagos Archipelago: Melting and magmatic evolution at the margins of a mantle plume, *J. Petrol.*, *46*(11), 2197–2224.
Geist, D. J., D. J. Fornari, M. D. Kurz, K. S. Harpp, A. Soule, M. Perfit, and A. M. Koleszar (2006), Submarine Fernandina: Magmatism at the leading edge of the Galápagos hot spot, *Geochem. Geophys. Geosyst.*, *7*, Q12007, doi:10.1029/2006GC001290.
Geldmacher, J., T. W. Höfig, F. Hauff, K. Hoernle, D. Garbe-Schönberg, and D. S. Wilson (2013), Influence of the Galápagos hotspot on the East Pacific Rise during Miocene superfast spreading, *Geology*, *41*(2), 183–186, doi:10.1130/G33533.1.
Georgen, J. E. (2014), Interaction of a mantle plume and a segmented mid-ocean ridge: Results from numerical modeling, *Earth Planet. Sci. Lett.*, *392*, 113–120, doi:10.1016/j.epsl.2014.01.035.
Gibson, S. A., and D. J. Geist (2010), Geochemical and geophysical mapping of lithospheric thickness variations beneath Galápagos, *Earth Planet. Sci. Lett.*, *300*, 275–286, doi:10.1016/j.epsl.2010.10.002.
Gibson, S. A., D. J. Geist, J. A. Day, and C. W. Dale (2012), Short wavelength heterogeneity in the Galápagos plume: Evidence from compositionally-diverse basalts on Isla Santiago, *Geochem. Geophys. Geosyst.*, *13*, Q09007, doi:10.1029/2012GC004244.
Goes, S., J. J. Armitage, N. Harmon, H. Smith, and R. S. Huismans (2012), Low seismic velocities below mid-ocean ridges: Attenuation vs. melt retention, *J. Geophys. Res.*, *117*, B12403, doi:10.1029/2012JB009637.
Graham, D. W., D. M. Christie, K. S. Harpp, and J. E. Lupton (1993), Mantle plume helium in submarine basalts from the Galápagos Platform, *Science*, *262*(5142), 2023–2026.
Graham, D. W., B. B. Hanan, J. E. Lupton, K. A. Hoernle, R. Werner, D. M. Christie and J. M. Sinton (2014), Helium isotope variations and mantle plume-spreading ridge interactions along the Galapagos Spreading Centre, in *The Galápagos: A Natural Laboratory for the Earth Sciences, Geophys. Monogr. Ser.*, edited by K. S. Harpp et al., vol. 204, pp. 393–414, AGU, Washington, D. C.
Gripp, A. E., and R. G. Gordon (2002), Young tracks of hotspots and current plate velocities, *Geophys. J. Int.*, *150*(2), 321–361, doi:10.1046/j.1365-246X.2002.01627.
Hall, P. S., and C. Kincaid (2003), Melting, dehydration, and the dynamics of off-axis plume-ridge interaction, *Geochem. Geophys. Geosyst.*, *4*(9), 8510, doi:10.1029/2003GC000567.
Hall, P. S., and C. Kincaid (2004), Melting, dehydration, and the geochemistry of off-axis plume-ridge interaction, *Geochem. Geophys. Geosyst.*, *5*, Q12E18, doi:10.1029/2003GC000667.
Hanan, B. B., and D. W. Graham (1996), Lead and helium isotope evidence from oceanic basalts for a common deep source of mantle plumes, *Science*, *272*(5264), 991–995, doi:10.1126/science.272.5264.991.
Harpp, K. S., and D. J. Geist (2002), Wolf-Darwin lineament and plume-ridge interaction in northern Galápagos, *Geochem. Geophys. Geosyst.*, *3*(11), 8504, doi:10.1029/2002GC000370.
Harpp, K. S., and W. M. White (2001), Tracing a mantle plume: Isotopic and trace element variations of Galápagos seamounts, *Geochem. Geophys. Geosyst.*, *2*(6), 1042, doi:10.1029/2000GC000137.
Harpp, K. S., D. J. Fornari, D. J. Geist, and M. D. Kurz (2003), Genovesa submarine ridge: A manifestation of plume-ridge interaction in the northern Galápagos Islands, *Geochem. Geophys. Geosyst.*, *4*(9), 8511, doi:10.1029/2003GC000531.
Harpp, K. S., V. D. Wanless, R. H. Otto, K. Hoernle, and R. Werner (2005), The Cocos and Carnegie Aseismic Ridges: A trace element record of long-term Plume–spreading center interaction, *J. Petrol.*, *46*(1), 109–133, doi:10.1093/petrology/egh064.
Harpp, K. S., D. Fornari, D. J. Geist, and M. D. Kurz (2014a), The geology and geochemistry of Isla Floreana, Galápagos: A different type of late stage ocean island volcanism, in *The Galápagos: A Natural Laboratory for the Earth Sciences, Geophys. Monogr. Ser.*, vol. 204, edited by K. S. Harpp, vol. 204, pp. 71–118, AGU, Washington, D. C.
Harpp, K. S., K. R. Wirth, R. Teasdale, S. Blair, L. Reed, J. Barr, J. Pistiner, and D. Korich (2014b), Plume-ridge interaction in the Galapagos: Perspectives from Wolf, Darwin and Genovesa Islands, in *The Galápagos: A Natural Laboratory for the Earth Sciences, Geophys. Monogr. Ser.*, edited by K. S. Harpp, pp. 285–334, AGU, Washington, D. C.
Hart, S. R., E. H. Hauri, L. A. Oschmann, and J. A. Whitehead (1992), Mantle plumes and entrainment: Isotopic evidence, *Science*, *256*(5056), 517–520.
Helfrich, K. R. (1995), Thermo-viscous fingering of flow in a thin gap: A model of magma flow in dikes and fissures, *J. Fluid Mech.*, *305*, 219–238, doi:10.1017/S0022112095004605.
Helo, C., M.-A. Longpré, N. Shimizu, D. A. Clague, and J. Stix (2011), Explosive eruptions at mid-ocean ridges driven by CO_2-rich magmas, *Nat. Geosci.*, *4*(4), 260–263, doi:10.1038/ngeo1104.
Hirth, G., and D. L. Kohlstedt (1996), Water in the oceanic upper mantle: Implications for rheology, melt extraction and the evolution of the lithosphere, *Earth Planet. Sci. Lett.*, *144*(1–2), 93–108.
Hoernle, K. A., R. Werner, J. P. Morgan, S. Garbe, J. Bryce and J. Mrazek (2000), Existence of complex spatial zonation in the Galápagos plume, *Geology*, *28*(5), 435–438.
Ingle, S., G. Ito, J. J. Mahoney, W. Chazey, J. M. Sinton, M. Rotella, and D. M. Christie (2010), Mechanisms of geochemical and geophysical variations along the western Galápagos spreading center, *Geochem. Geophys. Geosyst.*, *11*, Q04003, doi:10.1029/2009GC002694.
Ito, G., and J. Lin (1995a), Mantle temperature anomalies along the past and paleoaxes of the Galápagos spreading center as inferred from gravity analyses, *J. Geophys. Res.*, *100*(B3), 3733–3745, doi:10.1029/94JB02594.
Ito, G., and J. Lin (1995b), Oceanic spreading center–hotspot interactions: Constraints from along-isochron bathymetric and gravity anomalies, *Geology*, *23*(7), 657–660, doi:10.1130/0091–7613(1995).
Ito, G., and J. J. Mahoney (2005), Flow and melting of a heterogeneous mantle: 1. Method and importance to the geochemistry of ocean island and mid-ocean ridge basalts, *Earth Planet. Sci. Lett.*, *230*(1–2), 29–46, doi:10.1016/j.epsl.2004.10.035.
Ito, G., J. Lin, and C. W. Gable (1997), Interaction of mantle plumes and migrating mid-ocean ridges: Implications for the Galápagos plume-ridge system, *J. Geophys. Res.*, *102*(B7), 15,403–15,415.
Ito, G., Y. Shen, G. Hirth, and C. J. Wolfe (1999), Mantle flow, melting, and dehydration of the Iceland mantle plume, *Earth Planet. Sci. Lett.*, *165*(1), 81–96, doi:10.1016/S0012–821X(98)00216-7.

Ito, G., J. Lin, and D. W. Graham (2003), Observational and theoretical studies of the dynamics of mantle plume–mid-ocean ridge interaction, *Rev. Geophys.*, *41*(4), 1017, doi:10.1029/2002RG000117.

Ito, G. T., and T. Bianco (2014), Patterns in Galápagos magmatism arising from the upper mantle dynamics of plume-ridge interaction, in *The Galápagos: A Natural Laboratory for the Earth Sciences*, edited by K. S. Harpp, *Geophys. Monogr. Ser.*, pp. 245–262, AGU, Washington, D. C.

Jackson, M. G., S. R. Hart, A. E. Saal, N. Shimizu, M. D. Kurz, J. S. Blusztajn, and A. C. Skovgaard (2008), Globally elevated titanium, tantalum, and niobium (TITAN) in ocean island basalts with high $^{3}He/^{4}He$, *Geochem. Geophys. Geosyst.*, *9*, Q04027, doi:10.1029/2007GC001876.

Katz, R. F., and S. M. Weatherley (2012), Consequences of mantle heterogeneity for melt extraction at mid-ocean ridges, *Earth Planet. Sci. Lett.*, *335–336*, 226–237, doi:10.1016/j.epsl.2012.04.042.

Kincaid, C., G. Ito, and C. Gable (1995), Laboratory investigation of the interaction of off-axis mantle plumes and spreading centres, *Nature*, *376*(6543), 758–761, doi:10.1038/376758a0.

Kincaid, C., J.-G. Schilling and C. Gable (1996), The dynamics of off-axis plume-ridge interaction in the uppermost mantle, *Earth Planet. Sci. Lett.*, *137*(1–4), 29–43, doi:10.1016/0012–821X(95)00201-M.

Kingsley, R. H., and J.-G. Schilling (1998), Plume-ridge interaction in the Easter-Salas y Gomez seamount chain-Easter Microplate system: Pb isotope evidence, *J. Geophys. Res.*, *103*(B10), 24,159–24,177, doi:10.1029/98JB01496.

Kokfelt, T. F., C. Lundstrom, K. A. Hoernle, F. Hauff, and R. Werner (2005), Plume-ridge interaction studied at the Galápagos spreading center: Evidence from ^{226}Ra-^{230}Th-^{238}U and ^{231}Pa-^{235}U isotopic disequilibria, *Earth Planet. Sci. Lett.*, *234*(1–2), 165–187.

Koleszar, A. M., A. E. Saal, E. H. Hauri, A. N. Nagle, Y. Liang, and M. D. Kurz (2009), The volatile contents of the Galápagos plume: Evidence for H_2O and F open system behavior in melt inclusions, *Earth Planet. Sci. Lett.*, *287*(3–4), 442–452.

Kurz, M. D., and D. J. Geist (1999), Dynamics of the Galápagos hotspot from helium isotope geochemistry, *Geochim. Cosmochim. Acta*, *63*(23–24), 4139–4156.

Kurz, M. D., J. Curtice, D. Fornari, D. J. Geist, and M. Moreira (2009), Primitive neon from the center of the Galápagos hotspot, *Earth Planet. Sci. Lett.*, *286*(1–2), 23–34.

Kurz, M. D., K. S. Harpp, D. Geist, D. J. Fornari, J. Curtice, D. E. Lott, and W. J. Jenkins (2010), Noble gas tracers of mantle processes beneath the Galápagos archipelago (Invited), Abstract #V52A-05 presented at 2010 Fall Meeting, AGU, San Francisco, Calif.

Lenardic, A., M. A. Richards, and F. H. Busse (2006), Depth-dependent rheology and the horizontal length scale of mantle convection, *J. Geophys. Res.*, *111*, B07404, doi:10.1029/2005JB003639.

Maclennan, J., D. McKenzie, and K. Gronvöld (2001), Plume-driven upwelling under central Iceland, *Earth Planet. Sci. Lett.*, *194*(1–2), 67–82.

McDonough, W., and S.-S. Sun (1995), The composition of the Earth, *Chem. Geol.*, *120*, 223–253.

McKenzie, D. (1989), Some remarks on the movement of small melt fractions in the mantle, *Earth Planet. Sci. Lett.*, *95*(1–2), 53–72, doi:10.1016/0012–821X(89)90167-2.

McKenzie, D., J. Jackson, and K. Priestley (2005), Thermal structure of oceanic and continental lithosphere, *Earth Planet. Sci. Lett.*, *233*, 337–349.

Mittelstaedt, E., S. Soule, K. Harpp, D. Fornari, C. McKee, M. Tivey, D. Geist, M. D. Kurz, C. Sinton, and C. Mello (2012), Multiple expressions of plume-ridge interaction in the Galápagos: Volcanic lineaments and ridge jumps, *Geochem. Geophys. Geosyst.*, *13*, Q05018, doi:10.1029/2012GC004093.

Mittelstaedt, E., A. Soule, K. S. Harpp, and D. Fornari (2014), Variations in crustal thickness, plate rigidity and volcanic processes throughout the northern Galápagos volcanic province, in *The Galápagos: A Natural Laboratory for the Earth Sciences, Geophys. Monogr. Ser.*, pp. 263–284, AGU, Washington, D. C.

Morgan, W. J. (1978), Rodriguez, Darwin, Amsterdam, . . ., A second type of hotspot island, *J. Geophys. Res.*, *83*(B11), 5355–5360, doi:10.1029/JB083iB11p05355.

Naumann, T. R., and D. J. Geist (1999), Generation of alkalic basalt by crystal fractionation of tholeiitic magma, *Geology*, *27*(5), 423–426.

Paulson, A., and M. A. Richards (2009), On the resolution of radial viscosity structure in modelling long-wavelength postglacial rebound data, *Geophys. J. Int.*, *179*(3), 1516–1526, doi:10.1111/j.1365-246X.2009.04362.x.

Priestley, K., and D. McKenzie (2006), The thermal structure of the lithosphere from shear wave velocities, *Earth Planet. Sci. Lett.*, *244*(1–2), 285–301.

Ribe, N. M. (1996), The dynamics of plume-ridge interaction: 2. Off-ridge plumes, *J. Geophys. Res.*, *101*(B7), 16,195–16,204.

Ribe, N. M. and W. L. Delattre (1998), The dynamics of plume–ridge interaction—III. The effects of ridge migration, *Geophys. J. Int.*, *133*(3), 511–518, doi:10.1046/j.1365-246X.1998.00476.x.

Richards, M. A. (1991), Hotspots and the case for a high viscosity lower mantle, in *Glacial Isostasy, Sea-Level and Mantle Rheology*, edited by S. Roberto, K. Lambeck, and E. Boschi, pp. 571–587, Kluwer Acad., Dordrecht, Netherlands.

Richards, M. A., and R. W. Griffiths (1989), Thermal entrainment by deflected mantle plumes, *Nature*, *342*(6252), 900–902, doi:10.1038/342900a0.

Rudge, J. F., J. Maclennan, and A. Stracke (2013), The geochemical consequences of mixing melts from a heterogeneous mantle, *Geochim. Cosmochim. Acta*, *114*, 112–143, doi:10.1016/j.gca.2013.03.042.

Saal, A. E., M. D. Kurz, S. Hart, J. S. Blusztajn, G. D. Lane, K. Sims, and D. J. Geist (2000), U series isotopic variability in Galapagos lavas, evidence of a mildly buoyant plume, *Eos Trans. AGU*, *81*(48), Fall Meet. Suppl., Abstract V22C-03.

Saal, A. E., M. D. Kurz, S. R. Hart, J. S. Blusztajn, J. Blichert-Toft, Y. Liang, and D. J. Geist (2007), The role of lithospheric gabbros on the composition of Galápagos lavas, *Earth Planet. Sci. Lett.*, *257*, 391–406.

Schilling, J.-G., R. N. Anderson, P. Vogt (1976), Rare earth, Fe and Ti variations along the Galapagos spreading centre, and their relationship to the Galapagos mantle plume, *Nature*, *261*, 108–113.

Schilling, J.-G. (1991), Fluxes and excess temperatures of mantle plumes inferred from their interaction with migrating mid-ocean ridges, *Nature*, *352*(6334), 397–403, doi:10.1038/352397a0.

Schilling, J.-G., R. H. Kingsley and J. D. Devine (1982), Galápagos hot spot-spreading center system: 1. Spatial petrological and geochemical variations (83°W to 111°W), *J. Geophys. Res.*, *87*(B7), 5593–5610, doi:10.1029/JB087iB07p05593.

Schilling, J.-G., G. Thompson, R. Kingsley and S. Humphris (1985), Hotspot-migrating ridge interaction in the South Atlantic, *Nature*, *313*(5999), 187–191, doi:10.1038/313187a0.

Schilling, J.-G., D. Fontignie, J. Blichert-Toft, R. Kingsley and U. Tomza (2003), Pb-Hf-Nd-Sr isotope variations along the Galápagos spreading center (101°–83°W): Constraints on the dispersal of the Galápagos mantle plume, *Geochem. Geophys. Geosyst.*, *4*(10), 8512, doi:10.1029/2002GC000495.

Schutt, D. L., and K. Dueker (2008), Temperature of the plume layer beneath the Yellowstone hotspot, *Geology*, *36*(8), 623–626, doi:10.1130/G24809A.1.

Schutt, D. L., and C. E. Lesher (2006), Effects of melt depletion on the density and seismic velocity of garnet and spinel lherzolite, *J. Geophys. Res.*, *111*, B05401, doi:10.1029/2003JB002950.
Shorttle, O., J. Maclennan, and S. M. Jones (2010), Control of the symmetry of plume-ridge interaction by spreading ridge geometry, *Geochem. Geophys. Geosyst.*, *11*, Q0AC05, doi:10.1029/2009GC002986.
Sinton, J. M. (2003), Morphology and segmentation of the western Galápagos spreading center, 90.5°-98°W: Plume-ridge interaction at an intermediate spreading ridge, *Geochem. Geophys. Geosyst.*, *4*(12), 8515, doi:10.1029/2003GC000609.
Sleep, N. (2002), Ridge-crossing mantle plumes and gaps in tracks, *Geochem. Geophys. Geosyst.*, *3*(12), 8505, doi:10.1029/2001GC000290.
Sleep, N. (2008), Channeling at the base of the lithosphere during the lateral flow of plume material beneath flow line hot spots, *Geochem. Geophys. Geosyst.*, *9*, Q08005, doi:10.1029/2008GC002090.
Small, C. (1995), Observations of ridge-hotspot interactions in the Southern Ocean, *J. Geophys. Res.*, *100*(B9), 17,931–17,946, doi:10.1029/95JB01377.
Thoraval, C., and M. A. Richards (1997), The geoid constraint in global geodynamics: Viscosity structure, mantle heterogeneity models and boundary conditions, *Geophys. J. Int.*, *131*(1), 1–8, doi:10.1111/j.1365-246X.1997.tb00591.x.
Verma, S. P., and J.-G. Schilling (1982), Galápagos hot spot-spreading center system: 2. $^{87}Sr/^{86}Sr$ and large ion lithophile element variations (85°W-101°W), *J. Geophys. Res.*, *87*(B13), 10,838–10,856.
Vidito, C., C. Herzberg, E. Gazel, D. Geist, and K. Harpp (2013), Lithological structure of the Galápagos Plume, *Geochem. Geophys. Geosyst.*, *14*, 4214–4240, doi:10.1002/ggge.20270.
Villagómez, D. R., D. R. Toomey, E. E. Hooft, and S. C. Solomon (2007), Upper mantle structure beneath the Galápagos Archipelago from surface wave tomography, *J. Geophys. Res.*, *112*, B07303, doi:10.1029/2006JB004672.
Villagómez, D. R., D. R. Toomey, E. E. Hooft, and S. C. Solomon (2011), Crustal structure beneath the Galápagos Archipelago from ambient noise tomography and its implications for plume-lithosphere interactions, *J. Geophys. Res.*, *116*, B04310, doi:10.1029/2010JB007764.
Villagómez, D. R., D. R. Toomey, D. J. Geist, E. E. E. Hooft, and S. C. Solomon (2014), Mantle flow and multistage melting beneath the Galapagos hotspot revealed by seismic imaging, *Nat. Geosci.*, *7*, 151–156, doi:10.1038/ngeo2062.
Vogt, P. R., and G. L. Johnson (1975), Transform faults and longitudinal flow below the Midoceanic Ridge, *J. Geophys. Res.*, *80*(11), 1399–1428, doi:10.1029/JB080i011p01399.
Weatherley, S. M., and R. F. Katz (2010), Plate-driven mantle dynamics and global patterns of mid-ocean ridge bathymetry, *Geochem. Geophys. Geosyst.*, *11*, Q10003, doi:10.1029/2010GC003192.
Weatherley, S. M., and R. F. Katz (2012), Melting and channelized magmatic flow in chemically heterogeneous, upwelling mantle, *Geochem. Geophys. Geosyst.*, *13*, Q0AC18, doi:10.1029/2011GC003989.
Werner, R. (2003), Geodynamic evolution of the Galápagos hot spot system (Central East Pacific) over the past 20 m.y.: Constraints from morphology, geochemistry, and magnetic anomalies, *Geochem. Geophys. Geosyst.*, *4*(12), 1108, doi:10.1029/2003GC000576.
White, W. M., A. R. McBirney, and R. A. Duncan (1993), Petrology and geochemistry of the Galápagos Islands—Portrait of a pathological mantle plume, *J. Geophys. Res.*, *98*(B11), 19,533–19,563.
Wilson, D. S., and R. N. Hey (1995), History of rift propagation and magnetization intensity for the Cocos-Nazca spreading center, *J. Geophys. Res.*, *100*(B6), 10,041–10,056.
Wylie, J. J., and J. R. Lister (1995), The effects of temperature-dependent viscosity on flow in a cooled channel with application to basaltic fissure eruptions, *J. Fluid Mech.*, *305*, 239–261, doi:10.1017/S0022112095004617.